Crustal structure across the western Barents Sea from deep seismic and potential field data

Implications for Caledonian trends and subsequent basin formation

Iselin Aarseth

Thesis for the Degree of Philosophiae Doctor (PhD)
University of Bergen, Norway
2018

UNIVERSITY OF BERGEN

Crustal structure across the western Barents Sea from deep seismic and potential field data

Implications for Caledonian trends and subsequent basin formation

Iselin Aarseth

Thesis for the Degree of Philosophiae Doctor (PhD)
at the University of Bergen

2018

Date of defence: 24.05.2018

Year: 2018

Title: Crustal structure across the western Barents Sea from deep seismic and potential field data

Name: Iselin Aarseth

Print: Skipnes Kommunikasjon / University of Bergen

Preface to the thesis

This dissertation for the degree of philosophiae doctor (PhD) has been submitted to the Department of Earth Science at the University of Bergen. The project was supported by the Research Council of Norway FRINATEK program through BarPZ project 234153.

The candidate enrolled in the PhD program at the Department of Earth Science at the University of Bergen and the work presented in this thesis was carried out in the Geodynamics Group between January 2015 and December 2017. The research was supervised by Professor Rolf Mjelde (University of Bergen) and co-supervised by Associate Professor Asbjørn Johan Breivik (University of Oslo), Professor Jan Inge Faleide (University of Oslo) and Professor Ritske Huismans (University of Bergen).

Guide for Readers

The thesis follows an article-based format and is presented in three main parts. First, an introduction addressing the aims of the study, background, data and methods is provided. The main part of the thesis contains the result of the research presented as scientific paper that are published or submitted to peer-reviewed scientific journals. The last part is a synthesis of the study providing a brief summary and a discussion of the main result, implications, conclusions and perspectives for further work. References cited in the introduction and synthesis is given at the end of this thesis.

Acknowledgements

Firstly I would like to thank my main supervisor, Rolf Mjelde, for your support and guidance during these three years. Thanks for always having your door open. I thank Asbjørn Johan Breivik for indispensable help and support with Rayinvr and GMT. Thanks to Alexander Minakov for discussions and for sharing your experience in gravity and magnetic modeling, and to Jan Inge Faleide for discussions and knowledge about the geology of the Barents Sea. I also wish to thank Ritske Huismans for initiating the project and all my co-authors for your valuable input and suggestions that improved the papers.

Thanks to my friends and colleagues Thomas, Hallgeir, Kenneth, Ronny and Fabian for all the coffee breaks, jokes and for sharing both positive and negative experiences of the PhD life.

I also want to thank my family and friends for encouraging words and support during the last three years. A special thanks to my dad, Magnar, for encouraging me to take on this endeavor and for always believing in me.

Finally, I would like to thank Ingeborg for keeping me motivated and Petter for always being there for me. This thesis would not be possible without your support.

Iselin Aarseth

December 21st, 2017

'All models are wrong, but some are useful.'

- George Box

Abstract

The aim of this project is to map the deep crustal structure of the western Barents Sea in order to increase the understanding of how pre-existing structures related to the Caledonian orogeny and subsequent extensional collapse influenced Palaeozoic rift evolution. Modeling of ocean bottom seismometer data, combined with gravity and magnetic data have been utilized to generate large-scale models along three refraction seismic profiles acquired in 2014. The profiles cross the western Barents Sea with total length of more than 1450 km and include records from a total of 82 receivers. This thesis contains three papers that provide new constraints on the basement and basin configurations in the western Barents Sea.

Paper 1 discusses the nature of different basement domains and the eastern limit of the Caledonian suture. The paper presents a P-wave velocity and gravity model along a 650 km long transect. Lateral velocity changes in the crystalline crust are interpreted to represent the Caledonian suture between Laurentia and Barentsia. Additionally, a change in seismic reflectivity indicates a Caledonian suture through the Barents Sea, separating Baltica and Barentsia. Local deepening of Moho creates "root structures" that can be linked to Caledonian compressional deformation or a suture zone. Our model supports the existence of a separate NE-SW Caledonian trend into the central Barents Sea, branching off the N-S trending Svalbard Caledonides, implying the existence of Barentsia as an independent microcontinent between Laurentia and Baltica.

Paper 2 investigates Caledonian trends along a profile further south and provides new constraints of the proposed suture zones. Lateral velocity variations in the crystalline crust are interpreted as a transition from Caledonian basement in the west to Timanian basement in the east. Magnetic anomalies correlate well with high velocities and densities in the lower crust beneath Loppa High, suggesting that upper-crustal basement structures may not have significantly affected the magnetic anomaly

pattern, and may therefore not necessarily constrain the early post-Caledonian basin formation.

Paper 3 discusses the recent (2008-2016) earthquake sequence in Storfjorden south of Svalbard and its possible link to an old zone of weakness within Barentsia. A double magnetic anomaly is observed in the westernmost part of the model, coinciding with the location of a possible high-velocity body modeled in the lower crust. The positive magnetic anomalies are located in the proximity of the Storfjorden earthquake sequence, indicating that compositional and rheological variations in the crust could be related to the seismic activity. The distribution of earthquakes and fault plane solutions suggest the existence of a complex NE-SW oriented fault zone through Storfjorden, and we propose that this zone is linked to the heterogeneous crust in the western part of the model and that it represents old zones of weakness in the crystalline crust, possibly of Caledonian age. Regional and local stresses are most likely related to both thermal and post-glacial uplift that combined with the pre-existing zones of weakness in the crust could explain the recent seismic activity.

The research presented here provides new constraints on the crustal structure of the western Barents Sea and insights to large scale processes responsible for the post-Caledonian evolution of the Arctic region.

Authorship statement and list of publications

Paper 1: Crustal structure and evolution of the Arctic Caledonides: Results from controlled-source seismology.

Published in Tectonophysics 718, 9-24 (2017).

Aarseth, I., Mjelde, R., Breivik, A. J., Minakov, A., Faleide, J. I. Flueh, E., Huismans, R. S.

Paper 2: Crustal structure across the southwestern Barents Sea: Implications for Caledonian- and basin trends.

Submitted to Tectonophysics.

Aarseth, I., Mjelde, R., Breivik, A. J., Minakov, A., Faleide, J. I. Flueh, E., Huismans, R. S.

Paper 3: The Storfjorden earthquake sequence: reactivation of Caledonian zones of weakness?

Manuscript draft. To be submitted to Tectonophysics.

Aarseth, I., Hauge, B. E., Mjelde, R., Breivik, A. J., Minakov, A., Faleide, J. I. Flueh, E., Huismans, R. S.

Table 1: Authorship contributions.

Task	Paper 1	Paper 2	Paper 3
Data acquisition	Mjelde, Flueh and Minakov	Mjelde, Flueh and Minakov	Mjelde, Flueh and Minakov
OBS data processing	Aarseth and Breivik	Aarseth	Aarseth
Grav/mag processing	Minakov	Minakov	Minakov
OBS data interp. and modeling	Aarseth	Aarseth	Aarseth and Hauge
Grav/mag modeling	Aarseth and Minakov	Aarseth and Minakov	Aarseth
Text	Aarseth	Aarseth	Aarseth
Figures	Aarseth and Breivik	Aarseth and Breivik	Aarseth and Breivik
Manuscript discussion and review	All authors	All authors	All authors

Contents

1. Introduction

1.1 From orogeny to rifting: the plate tectonic cycle

The formation of large orogens and subsequent rifting of continental crust is a fundamental aspect in plate tectonics and forms part of the Wilson cycle. The periodicity of ocean formation and closure was summarized by Wilson (1972) and can be described in six steps (Fig. 1). The cycle begins with (1) **continental extension**, rifting and graben formation leading to continental break-up and formation of oceanic crust along a spreading center. This is followed by (2) development of a classic **ocean basin** with **passive continental margins** at both sides and a mid-oceanic ridge at the center. This is the present situation in the Barents Sea with the western margin forming a passive continental margin bordering the Atlantic Ocean, and will eventually be followed by (3) **subduction** of an oceanic plate underneath a continental plate. The precursor of the Atlantic Ocean, the Iapetus Ocean, was subducted beneath Baltica, leading to (4) **closure** of the ocean basin (e.g. the former Iapetus Ocean). The Caledonian orogeny culminated in (5) **continental collision** between Laurentia and Baltica in Silurian-Devonian times. Following the (6) **orogenic collapse** of the Caledonides, the cycle starts over again. The continental crust underlying the Barents Sea region has been affected by several orogenic events that leave its marks in the form of structural zones of weakness within the crystalline crust. The subsequent rifting and basin formation in the western Barents Sea is inferred to be influenced by structures inherited from the Caledonian orogeny. In the Barents Sea, these structures are covered by younger sedimentary rocks and the early post-Caledonian evolution is not well understood and forms the main topic of this thesis.

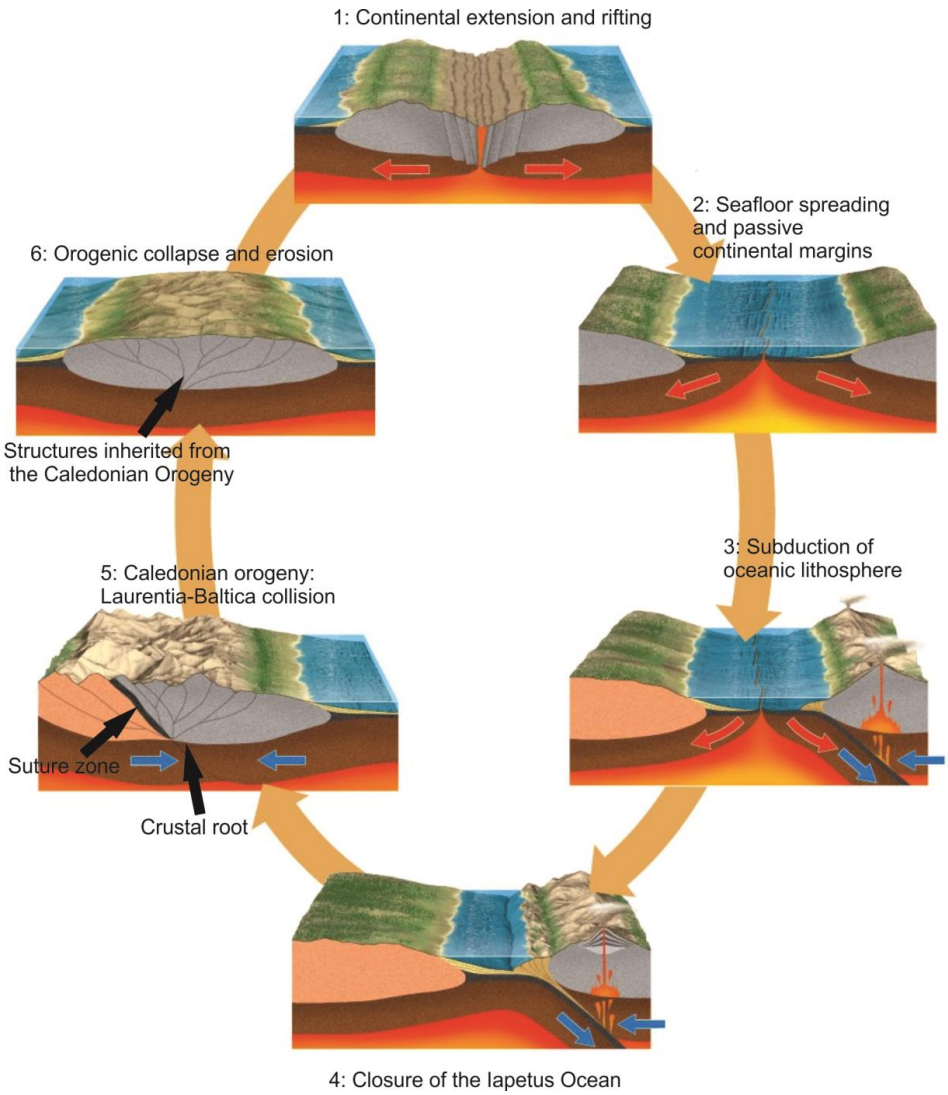

***Figure 1**: Schematic illustration of the Wilson cycle (Wilson, 1972) with examples from the Barents Sea. See text for further explanation.*

1.2 Study area and geological framework

This thesis provides a study of the crustal structure of the western Barents Sea, located in the northwestern corner of the Eurasian plate (Fig. 2). The Barents Sea borders the Norwegian-Greenland Sea in the west, Svalbard and Franz Josef Land in the north, Novaya Zemlya in the east and to the coast of Norway and Russia in the south and is one of the largest continental shelf areas on Earth.

The western Barents Sea has been affected by several orogenic events and rifting episodes. The Timanide Orogen (Precambrian-Cambrian) extends from the southern Polar Urals to the Varanger Peninsula in northern Norway, where it is truncated by later Caledonian deformation (Pease et al., 2014). The Caledonian Orogeny (Silurian-Devonian) culminated in the collision between Laurentia and Baltica following the closure of the Iapetus Ocean (e.g. Roberts and Gee, 1985; Gee et al., 2006; Gasser, 2014). The westernmost part of the Barents Sea in underlain by Caledonian basement, but the eastern limit of Caledonian deformation and the location of the Caledonian suture is heavily debated (e.g. Gudlaugsson et al., 1998; Breivik et al., 2005; Gee et al., 2006; Barrère et al., 2009; Henriksen et al., 2011a; Gernigon and Brönner, 2012; Gernigon et al., 2014) and will be discussed in section 1.3 and in the synthesis. Caledonian rocks are presently exposed mainly in the British Isles, Scandinavia, Greenland and Svalbard. On the Barents Shelf, Caledonian rocks are covered by a thick succession of late Palaeozoic to Cenozoic sediments and the structure of the crystalline crust related to the Caledonian orogeny can only be revealed from geophysical methods or borehole data. The Scandinavian Caledonides strike NE-SW in northern Norway, while the Svalbard Caledonides strike mainly N-S. Various interpretations exist to link these two trends and will be discussed in this thesis.

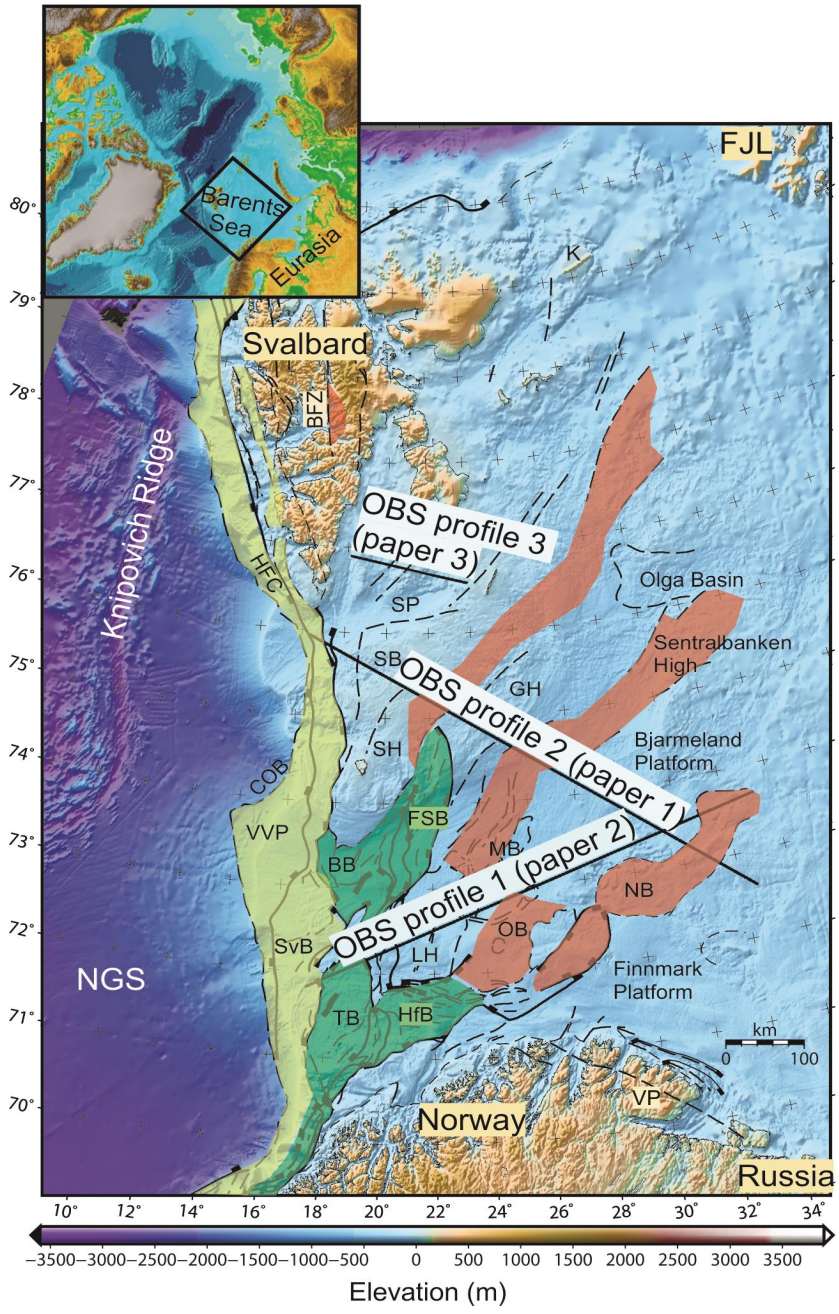
Barents Sea
Eurasia
FJL
K
Svalbard
BFZ
Knipovich Ridge
HFC
OBS profile 3 (paper 3)
SP
Olga Basin
Sentralbanken High
SB
OBS profile 2 (paper 1)
GH
Bjarmeland Platform
SH
COB
VVP
FSB
MB
BB
OBS profile 1 (paper 2)
NB
OB
SvB
LH
Finnmark Platform
NGS
TB
HfB
km
0
100
VP
Norway
Russia
80°
79°
78°
77°
76°
75°
74°
73°
72°
71°
70°
10°
12°
14°
16°
18°
20°
22°
24°
26°
28°
30°
32°
34°
−3500 −3000 −2500 −2000 −1500 −1000 −500 0 500 1000 1500 2000 2500 3000 3500
Elevation (m)

***Figure 2 (previous page)**: Bathymetry of the Barents Sea (from Jakobsson et al., 2012) and target areas of this PhD project. Fault positions from Faleide et al. (1993), outline of basin and highs from Gabrielsen et al. (1990). COB: continent-ocean boundary from Breivik et al. (1999). Age of rift basins from Faleide et al. (2010): red: Late Palaeozoic, green: Late Jurassic – Early Cretaceous, yellow: Late Cretaceous – Palaeocene. BB: Bjørnøya Basin, BFZ: Billefjorden Fault Zone, FJL: Franz Josef Land, FSB. Fingerdjupet Sub Basin, GH: Gardarbanken High, HfB: Hammerfest Basin, HFC: Hornsund Fault Complex, K: Kvitøya, LH: Loppa High, MB: Maud Basin, NB: Nordkapp Basin, NGS: Norwegian Greenland Sea, OB: Ottar Basin, SB: Sørkapp Basin, SvB: Sørvestsnaget Basin, SH: Stappen High, SP: Svalbard Platform, TB: Tromsø Basin, VP: Varanger Peninsula, VVP: Vestbakken Volcanic Province.*

The development of the western Barents Sea following the collapse of the Caledonian Orogeny (Fig. 3) have been dominated by episodic rifting from Paleozoic to Cenozoic times (e.g. Doré, 1991; Faleide et al., 1993). Early post-Caledonian rifting created Devonian basins on Spitsbergen, but whether Devonian basin formation also occurred is the Barents Sea is uncertain. Carboniferous rifting formed basins in the western Barents Sea (e.g. Nordkapp and Ottar basins) that accumulated large volumes of evaporites (Breivik et al., 1995). Late Jurassic to Early Cretaceous rifting resulted in deep and narrow basins (e.g. Bjørnøya and Tromsø basins) close to the present-day continent-ocean-boundary (Faleide et al., 1993; Breivik et al., 1998; Fig. 2).

The Ellesmerian Orogeny extends from Ellesmerian fold belt of North Greenland and Ellesmere Island in northern Canada to northwestern Svalbard, where it is known as the Svalbardian event. This orogenic event is associated with east-west compression in the earliest Carboniferous (Piepjohn et al., 2000). Svalbard and the northern Barents Sea were not affected by the Late Jurassic – Early Cretaceous rifting that formed the deep basins of the southwestern Barents Sea (Faleide et al., 1993). However, the region experienced widespread Early Cretaceous magmatism related to the High Arctic Large Igneous Province (e.g. Minakov et al., 2012, 2017). Magmatic intrusions are widespread across Svalbard and Franz Josef Land and the emplacement of these were probably controlled by Palaeozoic rift structures that were reactivated

in the Early Cretaceous (Minakov et al., 2012). The Palaeogene Eurekan/Spitsbergen fold belt is related to plate boundary geometry and change of spreading directions in the early Cenozoic (Piepjohn et al., 2016), when the northward movement of Greenland resulted in compressional deformation on Ellesmere Island and transpressional deformation on Spitsbergen (Leever et al., 2011). The Eurekan fold belt is linked to Spitsbergen via northern Greenland (Petersen et al., 2016). The western Barents Sea and Svalbard experienced strong uplift and erosion both during Early Cretaceous (Drachev and Saunders, 2006; Worsley, 2008) and through several Pliocene/Pleistocene post-glacial phases (Dimakis et al., 1998; Henriksen et al., 2011b).

It has long been recognized that inherited basement structures from the Caledonian Orogeny and older events have a tectonic influence on the structural configuration of rifts and the development of the continental margin and sedimentary basins in the southwestern Barents Sea (e.g. Harland and Gayer, 1972; Gabrielsen, 1984; Doré, 1991; Ritzmann and Faleide, 2007). However, the deep structure of the Late Palaeozoic basins and their relation to the Caledonian orogeny remains unresolved in most of the western Barents Sea due to sparse distribution of wide-angle seismic data and poor resolution of multi-channel seismic reflection data below the Permian sequence. A good understanding of both the basin and basement configuration is crucial for understanding the complex relationships between inherited structures and subsequent rifting and basin evolution.

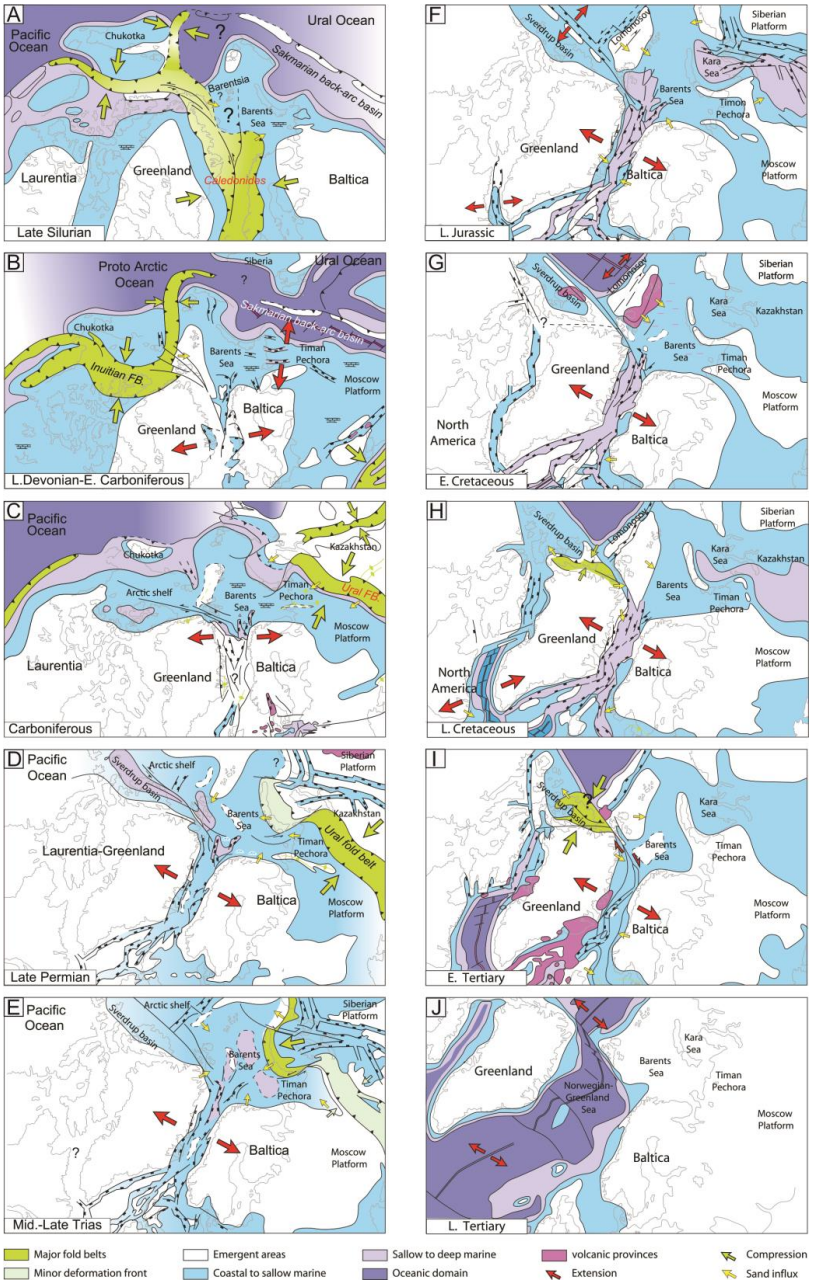

***Figure 3**: Geodynamic evolution of the North Atlantic and Arctic regions. Figures A-D illustrates the Caledonian orogeny and early post-Caledonian rifting that represents the main research question in this thesis. Modified from Smelror et al., 2009.*

1.3 Research questions

The present day large-scale structure of the Barents Shelf can roughly be divided into two major geological provinces: the eastern Barents Sea and the western Barents Sea. From geophysical data the configuration of the top crystalline crust in the Barents Sea reveals structural highs and lows of different wavelength from west to east, implying that the regions are underlain by different basement domains (e.g. Ritzmann and Faleide, 2007; Marello et al., 2013; Klitzke et al., 2016; Faleide et al., 2017; Fig. 4). The geology of the western Barents Sea is to a large extent controlled by the Caledonian Orogeny, post-Caledonian rifting and continental break-up (e.g. Talwani and Eldholm, 1977; Gabrielsen et al., 1984; Gee et al., 2006; Faleide et al., 2008). However, the eastern limit of the Caledonian suture and deformation front is not well resolved (e.g. Gudlaugsson et al., 1998; Breivik et al., 2005; Gee et al., 2006; Barrère et al., 2009; Henriksen et al., 2011a). In order to increase the understanding of the early post-Caledonian evolution of the region, the primary objective of this thesis is to:

1. Locate the main Caledonian suture and deformation front in the western Barents Sea.

A separate NE-SW Caledonian suture extending into the central Barents Sea, branching off from the northerly trending Svalbard Caledonides have been suggested (e.g. Gudlaugsson et al., 1998; Breivik et al., 2002). This implies the existence of Barentsia as an independent microcontinent between Laurentia and Baltica, however the limits of the Barentsia microcontinent is not well constrained and the present study aims to:

2. Locate the postulated Baltica-Barentsia suture and constrain the southern boundary of the Barentsia microcontinent.

The crystalline crust beneath the southwestern Barents Sea is believed to represent the northward continuation of the Caledonides in northern Norway (Breivik et al.,

1998, 2005; Ritzmann and Faleide, 2007; Marello et al., 2013). A series of NE-SW trending nappes have been mapped in the onshore fold and thrust belt, a trend that also dominates the crustal configuration in the southwestern Barents Sea (Faleide et al., 1993; Breivik et al., 1998; Ritzmann and Faleide, 2007). However, this configuration has recently been challenged by high-resolution magnetic data, suggesting that Caledonian structures turn from a NE-SW orientation in northern Norway to NNW-SSE or NW-SW across the Nordkapp Basin and Bjarmeland Platform, and continues northwards to Svalbard (Gernigon and Brönner, 2012; Gernigon et al., 2014, Fig. 2). Therefore, this study further aims to:

3. Determine the trend of early post-Caledonian rift basins.

An earthquake sequence was initiated by the $M_w = 6.1$ Storfjorden, Svalbard event on 21 February 2008. The earthquake distribution and fault plane solutions suggest that the seismic activity is primarily related to NE-SW striking faults; in contrast to the major N-S oriented faults mapped onshore Svalbard. NE-SW striking faults in Storfjorden have not been identified by seismic data and we aim to:

4. Map the crustal structure across the Storfjorden earthquake sequence in order to identify structures associated with the recent seismic activity and its possible link to Caledonian trends.

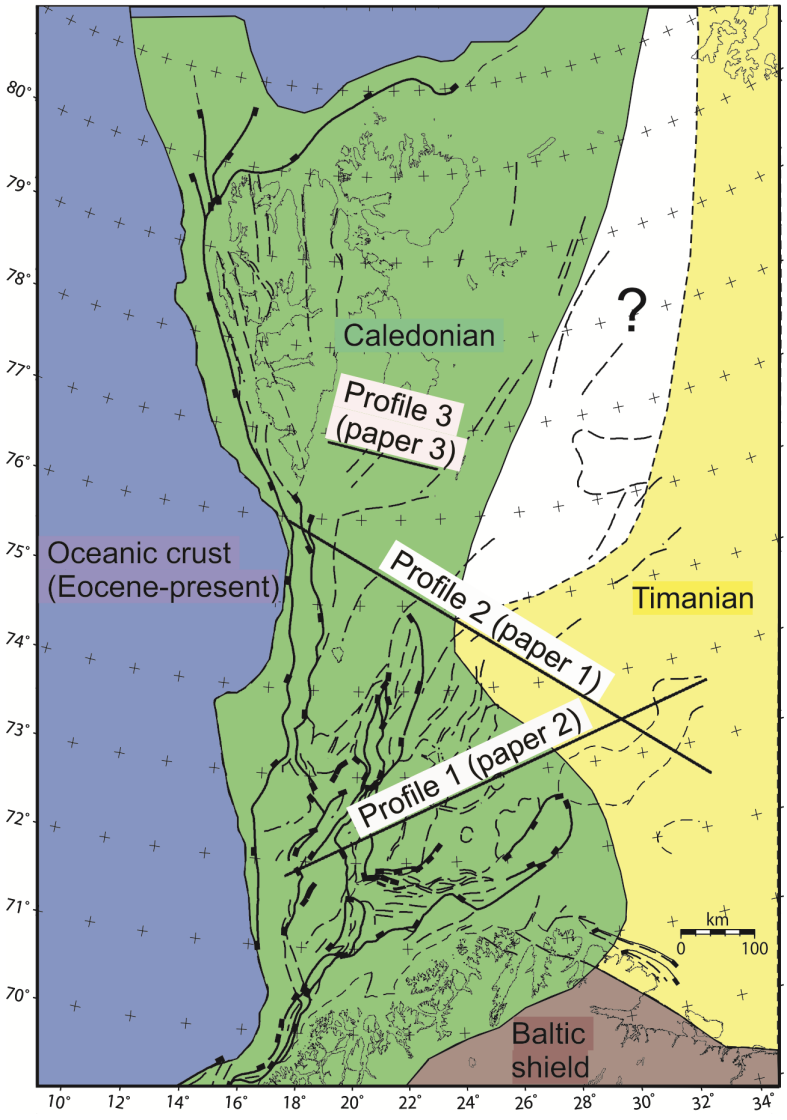

***Figure 4**: Basement domains in the western Barents Sea. White areas are unconstrained. Modified from Faleide et al., 2017.*

1.4 Data and methods

A regional ocean bottom seismometer (OBS) survey was conducted in the western Barents Sea during July-August 2014 using the R/V Håkon Mosby as part of the PETROMAKS project (Minakov et al., 2014). OBS stations were deployed with a spacing distance of 15-20 km along two regional profiles (Profile 1 and 2, Figs. 2, 4), across the western Barents Sea, and along a shorter profile (Profile 3, Figs. 2, 4) in Storfjorden south of Svalbard. Air-gun shots were fired every 200 meters using four equal-sized air guns with a total volume of 78.66 liters.

Profile 1 and 2 were acquired along existing multichannel seismic lines. Gravity-, magnetic-, and bathymetry data were recorded continuously along all profiles using a LaCoste and Romberg shipboard gravity meter, a marine proton magnetometer and an echo-sounder, respectively. The dataset from 2014 forms the foundation for this thesis and has been used to study the crustal structure of the western Barents Sea.

The main advantage of wide-angle seismic surveys, such as OBS surveys, is the ability to map deep sedimentary and crustal structures through layers of volcanic, intrusive or carbonate rocks (e.g. Mjelde et al., 1992, 1996). The high acoustic impedance of such layers makes imaging beneath them difficult by use of the conventional multichannel reflection technique. Another advantage of placing the receivers on the ocean floor is the possibility to record S-waves. This can be done using horizontally mounted geophones, in addition to the vertical geophones used for P-wave analysis. Multichannel reflection seismic (MSC) data has better resolution than wide-angle seismic data in the upper (sedimentary) part of the records. Where available, MCS data was used in the initial model building to constrain the shallow part of the models.

The recorded OBS data have been modeled using the forward and inverse ray-tracing method described by Zelt and Smith (1992). Calculation of travel-times is done by integrating the inverse of the velocity along ray paths. Snell's law is applied at layer

boundaries and the 2-D ray-tracing equations are solved numerically, assuming an isotropic medium. The velocity model may be updated manually (forward modeling) or by inversion. The inverse problem is solved using a damped least squares approach. The model is parameterized by linear interpolation between velocity nodes at the top and bottom of each layer, and between adjacent velocity nodes laterally in a layer.

Velocity models based on travel-times recorded on widely spaced OBS stations are non-unique and integrating data from different sources results in more robust models. To achieve this, gravity- (paper 1, 2 and 3) and magnetic data (Paper 2 and 3) have been combined with the seismic models. Modeling of potential field data was done using Geosoft Oasis montaj software (Geosoft Inc. 2008).

1.5 Contributions at scientific meetings

Aarseth, I., Mjelde, R., Breivik, A. J., Minakov, A., Huismans, R. S., Faleide, J. I., 2016. Barents Sea Paleozoic basement and basin configurations: Crustal structure from deep seismic and potential field data (Poster) In: EGU General Assembly, 17-22 April, 2016, Vienna, Austria.

Shulgin, A., Aarseth, I., Faleide, J. I., Mjelde, R., Huismans, R., 2016. The Western Barents Sea: where is the Caledonian Deformation Front? (Poster) In: EGU General Assembly, 17-22 April, 2016, Vienna, Austria.

Aarseth, I., Mjelde, R., Breivik, A. J., Minakov, A., Huismans, R. S., Faleide, J. I., 2016. Barents Sea Paleozoic basement and basin configurations: Crustal structure from deep seismic and potential field data (Poster) In: Seismix 2016, International Seismix Symposium, 15-20 May, 2016, Aviemore, Scotland.

Aarseth, I., Mjelde, R., Breivik, A. J., Minakov, A., Huismans, R. S., Faleide, J.I., 2016. Barents Sea Paleozoic basement and basin configurations: Crustal structure from deep seismic and potential field data (Oral) In: AGU Fall Meeting, 12-16 December, 2016, San Francisco, USA.

2. Manuscript compilation

Paper 1:

Crustal structure and evolution of the Arctic Caledonides: Results from controlled-source seismology

Iselin Aarseth[a*], Rolf Mjelde[a], Asbjørn Johan Breivik[b], Alexander Minakov[b], Jan Inge Faleide[b], Ernst Flueh[c], Ritske S. Huismans[a]

[a] Department of Earth Science, University of Bergen, Allégaten 41, N-5007 Bergen, Norway

[b] Department of Geosciences, University of Oslo, P.O. box 1047, Blindern, N-0316 Oslo Norway

[c] GEOMAR, Wischhofstrasse 1-3, 24148 Kiel, Germany

Published in Tectonophysics

Tectonophysics 718 (2017) 9–24

Contents lists available at ScienceDirect

Tectonophysics

journal homepage: www.elsevier.com/locate/tecto

Crustal structure and evolution of the Arctic Caledonides: Results from controlled-source seismology

Iselin Aarseth [a,*], Rolf Mjelde [a], Asbjørn Johan Breivik [b], Alexander Minakov [b], Jan Inge Faleide [b], Ernst Flueh [c], Ritske S. Huismans [a]

[a] Department of Earth Science, University of Bergen, Allégaten 41, N-5007 Bergen, Norway
[b] Department of Geosciences, University of Oslo, PO Box 1047, Blindern, N-0316 Oslo, Norway
[c] GEOMAR, Wischhofstrasse 1-3, 24148 Kiel, Germany

ARTICLE INFO

Article history:
Received 17 November 2016
Received in revised form 31 March 2017
Accepted 20 April 2017
Available online 22 April 2017

Keywords:
Ocean bottom seismometers
Crustal structure
Caledonian orogeny
Svalbard

ABSTRACT

The continuation of the Caledonides into the Barents Sea has long been a subject of discussion, and two major orientations of the Caledonian deformation fronts have been suggested: NNW-SSE striking and NE-SW striking. A regional NW-SE oriented ocean bottom seismic profile across the western Barents Sea was acquired in 2014. In this paper we map the crust and upper mantle structure along this profile in order to discriminate between different interpretations of Caledonian structural trends and orientation of rift basins in the western Barents Sea. Modeling of P-wave travel times has been done using a ray-tracing method, and combined with gravity modeling. The results show high P-wave velocities (4 km/s) close to the seafloor, as well as localized sub-horizontal high velocity zones (6.0 km/s and 6.9 km/s) at shallow depths which are interpreted as magmatic sills. Refractions from the top of the crystalline basement together with reflections from the Moho give basement velocities from 6.0 km/s at the top to 6.7 km/s at the base of the crust. P-wave travel time modeling of the OBS profile indicate an eastwards increase in velocities from 6.4 km/s to 6.7 km/s at the base of the crystalline crust, and the western part of the profile is characterized by a higher seismic reflectivity than the eastern part. This change in seismic character is consistent with observations from vintage reflection seismic data and is interpreted as a Caledonian suture extending through the Barents Sea, separating Barentsia and Baltica. Local deepening of Moho (from 27 km to 33 km depth) creates "root structures" that can be linked to the Caledonian compressional deformation or a suture zone imprinted in the lower crust. Our model supports a separate NE-SW Caledonian trend extending into the central Barents Sea, branching off from the northerly trending Svalbard Caledonides, implying the existence of Barentsia as an independent microcontinent between Laurentia and Baltica.

1. Introduction

The Barents Sea is located in the northwestern corner of the Eurasian continent (Fig. 1) where the assembly of the crystalline basement is related to the mid-Palaeozoic Caledonian orogeny (e.g. Roberts and Gee, 1985). Early post-Caledonian extension created Devonian basins on Svalbard, but it is unknown how this phase affected the offshore areas. Late Palaeozoic rifting in the Barents Sea formed basins that accumulated large amounts of evaporite deposits, whereas Mesozoic rifting events formed major Cretaceous basins followed by Cenozoic breakup and opening of the Northeast Atlantic (Roberts and Gee, 1985; Gabrielsen et al., 1990; Faleide et al., 2008; Gee et al., 2008; Smelror et al., 2009). It has long been recognized that Caledonian and older basement structures have influenced subsequent basin development and structural configuration in the Barents Sea (Harland and Gayer, 1972; Gabrielsen, 1984; Doré, 1991; Ritzmann and Faleide, 2007, Fig. 2). Due to petroleum exploration in the southwestern Barents Sea the structures of the main Mesozoic grabens, highs and platforms are fairly well known (e.g. Gabrielsen et al., 1990; Faleide et al., 1993; Breivik et al., 1998; Smelror et al., 2009; Henriksen et al., 2011a). The deep structure of the Late Palaeozoic basins and their relationship to the Caledonian orogeny still remains unclear in most of the western Barents Sea due to sparse distribution of wide-angle seismic data and poor resolution of multi-channel seismic (MCS) reflection data below the Permian sequence (Breivik et al., 2005). Ziegler (1988) proposed that the Scandinavian Caledonides extend northwestward linking up with the N—S trending Caledonides of Svalbard. Later interpretations involve two branches of the Caledonides, one through the eastern Barents Sea, and one through Spitsbergen (Gudlaugsson et al., 1998; Breivik et al., 2005; Henriksen et al., 2011a). Others consider only the eastern branch through the Barents Sea to be the suture (Doré, 1991; Harland et al., 1997; Gee et al., 2006, Fig. 2).

* Corresponding author.
E-mail address: iselin.aarseth@uib.no (I. Aarseth).

http://dx.doi.org/10.1016/j.tecto.2017.04.022
0040-1951/

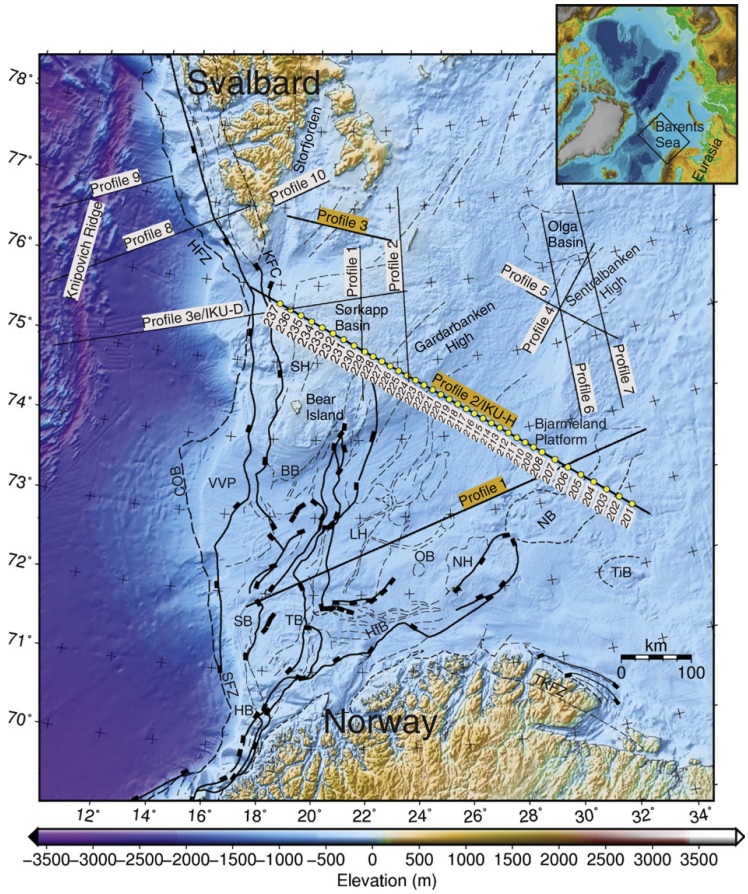

Fig. 1. Location the modeled Profile 2 with OBS locations marked by yellow dots. Profiles 1 and 3 from the 2014 survey are also shown. Bathymetry is taken from Jakobsson et al. (2012) fault positions from Faleide et al. (1993), outline of basin and highs from Gabrielsen et al. (1990). COB: continent-ocean boundary from Breivik et al. (1999) BB: Bjørnøya Basin, HB: Harstad Basin, HfB: Hammerfest Basin, HFZ: Hornsund Fault Zone, KFC: Knølegga Fault Complex, LH: Loppa High, NB: Nordkapp Basin, NH: Norsel High, OB: Ottar Basin, SB: Sørvestsnaget Basin, SH: Stappen High, TB: Tromsø Basin, TiB: Tiddlybanken Basin, TKFZ: Trollfjorden-Komagelva Fault Zone, VVP: Vestbakken Volcanic Province.

Further, it has been proposed that the Late Palaeozoic rifting in the southwestern Barents Sea developed in a north-easterly direction, following the inherited Caledonian structural grain, with a fan shaped distribution of rift basins and intra-basinal highs with orientations ranging from north-easterly in the main rift zone to northerly at the present continental margin in the west (e.g. Gudlaugsson et al., 1998; Breivik et al., 2005; Ritzmann and Faleide, 2007). However, based on new high quality aeromagnetic data covering the southwestern Barents Sea, Gernigon and Brönner (2012) and Gernigon et al. (2014) suggest that the sub-Permian basins and underlying basement grain have a dominantly NNW-SSE orientation and that Caledonian extensional collapse and subsequent rift evolution follow this trend. Contrary to previous interpretations the magnetic data do not recognize a NE-SW inherited Caledonian structural trend through the Barents Sea.

In areas where the deeper parts of the crust are difficult to image by conventional multi-channel seismic reflection data, wide-angle seismic experiments provide valuable information (e.g. Breivik et al., 2002). In 2014, three ocean bottom seismometer (OBS) profiles were acquired in the western Barents Sea (Minakov et al., 2014, Figs. 1, 2), crossing the proposed trends of Caledonian structures and Late Palaeozoic rifts. The P-wave velocity- and gravity model along OBS Profile 2 are presented in this paper. The profile is 650 km long and has a NW-SE orientation, crossing the western Barents Sea from the Stappen High area north of Bjørnøya to the Nordkapp Basin. The primary objective of this paper is to investigate how pre-existing structures inherited from the Caledonian orogeny and subsequent Devonian extensional collapse in the western Barents Sea influenced subsequent Palaeozoic rift evolution.

2. Geological setting

Four major orogenic events have influenced the geology of the Barents Sea area: the Timanian (Ediacaran), Caledonian (Mid Silurian–Early Devonian) (Fig. 2), Uralian (Early Carboniferous–Late Permian/Triassic) and Eurekan orogens (Early Cenozoic). During the Timanian orogeny terranes accreted against the present-day northeastern margin of Baltica. The Timanian structural trend generally has a NW-SE orientation and extends into the South Barents Basin (Olovyanishnikov et al., 1997; Roberts and Siedlecka, 2002), but how far north and west these trends extend is uncertain. NW trending Timanian structures are

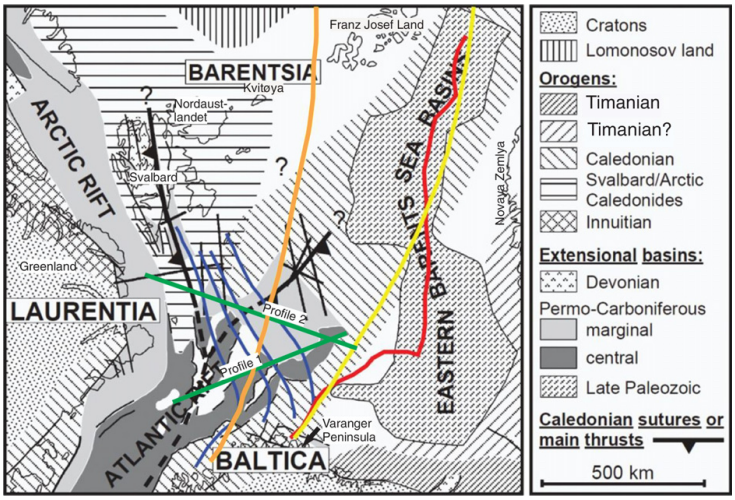

Fig. 2. Caledonide model from Gudlaugsson et al. (1998) compared with different interpretations of Caledonian structural trends. Black: OBS profiles modeled by Breivik et al. (2002, 2003 and 2005) and proposed Caledonian suture zones (Breivik et al., 2005). Orange: Proposed Caledonian suture (Gee et al., 2006). Yellow: Proposed Caledonian deformation front (Gee et al., 2006). Red: Proposed Caledonian deformation front (Henriksen et al., 2011a). Blue: Prolongation of Caledonian thrusts (Barrère et al., 2009; Gernigon and Brönner, 2012; Gernigon et al., 2014). Green: OBS Profiles 1 and 2 from this study. In the original figure Timanian was referred to as Baikalian.

exposed on the Varanger Peninsula in northernmost Norway (e.g. Roberts and Olovyanishnikov, 2004).

The Caledonian orogeny started in the Early Ordovician and culminated with the collision of Laurentia and Baltica in mid Silurian to Early Devonian time with the closure of the Iapetus Ocean (e.g. Gee et al., 2008). The Svalbard Archipelago comprises at least three crustal blocks and different hypotheses have been proposed for the Caledonian terrain assembly (Harland et al., 1997; Gee and Teben'kov, 2004; Cocks and Torsvik, 2011). The western terrains have Laurentian affinities (e.g. Harland et al., 1997), but the eastern part of Svalbard has been interpreted as an independent microcontinent between Laurentia and Baltica (Gudlaugsson et al., 1998; Torsvik et al., 2001; Breivik et al., 2002). The Uralian orogeny affected mostly the Eastern Barents Sea region during the collision between Laurussia (Laurentia and Baltica) and Siberia, with the closure of the Uralian Ocean (Churkin et al., 1981). Early Eocene compression formed the western Spitsbergen fold-and-thrust belt (e.g. Leever et al., 2011) during the Eurekan orogeny.

The complex structural framework of the Barents Shelf basement is a result of these collisional events. The Caledonian orogeny was followed by extensional collapse and Devonian graben formation. Post-orogenic sediments were deposited during the late Silurian-Devonian and compressively deformed in the Late Devonian tectonic phase referred to as the Svalbardian or Ellesmerian Event (Gee et al., 2008; Bergh et al., 2011; Blinova et al., 2013). Devonian rocks have mainly been preserved in north-south trending graben structures in Spitsbergen. Carboniferous rifting resulted in formation of several basins (e.g. Nordkapp Basin, Bjørnøya Basin, Tromsø Basin, Tiddlybanken Basin, Fig. 1) that collected large volumes of evaporites during the Late Carboniferous and Early Permian (Faleide et al., 1984; Gudlaugsson et al., 1998). Regional subsidence was established by the Early Permian and continued into the Triassic with deposition of clastic marine sediments. Rifting in the Middle Jurassic to Early Cretaceous created deep sedimentary basins and was followed by Early Cenozoic margin formation, opening of the Norwegian–Greenland Sea and the onset of seafloor spreading (Faleide et al., 1993). Early Cretaceous magmatism has affected areas northeast (e.g. Minakov et al., 2012) and south of Svalbard (Grogan et al., 2000; Breivik et al., 2005; Polteau et al., 2016) forming parts of the High Arctic Large Igneous Province (HALIP).

From mid-Miocene time to the present, the western Barents Sea has been regionally uplifted and eroded (Dengo and Røssland, 1992; Dimakis et al., 1998; Ohm et al., 2008; Henriksen et al., 2011b). Between 1500 m and 3200 m of the sedimentary sequence have been removed in our study area, leaving Triassic rocks close to the seafloor across the Bjarmeland Platform (Gudlaugsson et al., 1987) and only minor occurrences of Cretaceous sequences e.g. in the Nordkapp Basin (Faleide et al., 1984). The present western Barents Sea is dominated by a complex system of grabens and half-grabens, while the eastern Barents Sea consists of a single, much larger N—S trending sag basin. This structural difference implies that the eastern and the western Barents Sea are underlain by different basement domains and structural grains, and there could also be variations in tectono-magmatic and metamorphic processes from west to east (e.g. Gac et al., 2012).

3. Data and methods

3.1. Data acquisition

OBS data were acquired using the research vessel Håkon Mosby during the summer of 2014 by the University of Bergen (UiB) in cooperation with the University of Oslo (UiO) and GEOMAR. These comprise two regional profiles in the western Barents Sea and a shorter profile in Storfjorden south of Svalbard. Gravity-, magnetic-, and bathymetry data were recorded continuously along the profiles using a LaCoste-Romberg shipboard gravity meter, a marine proton magnetometer and an echo sounder, respectively. Additionally, single-channel streamer data were acquired during seismic shooting. Four equal-sized airguns with a total volume of 78.66 L (4800 in.^{3}) were fired every 200 m (approx. 80 s) along each profile. The data were recorded by digital GEOMAR Ocean Bottom Seismometers recording both P-wave (vertical geophone and hydrophone) and S-waves (two orthogonal horizontal geophones). Navigation is based on the Differential Global Positioning System (DGPS). Profile 2 was shot in two segments where the instruments were redeployed from one segment to the other, each containing 20 OBSs deployed at a typical distance of 15–20 km, with 3 OBSs overlapping between the segments. Each segment gave a seismic

record 394.6 km (NE) and 395.4 km (SE) long, respectively. With an overlap of 128.7 km the total length of the profile is 661.3 km.

3.2. Data processing

Preprocessing of the seismic data was done at GEOMAR, including cutting raw data into traces of 60 s, adjusting for instrumental clock drift, tieing to navigation, trace normalization and conversion to SEG-Y format. The OBS positions were then corrected for physical instrument drift. Further processing was done at UiB/UiO, including band pass filtering (4–16 Hz), spiking deconvolution (to compress the wavelet and suppress ringing) and automatic gain control (1 s window) to boost the far-offset signals. A reduction velocity of 8 km/s was applied in order to compress the time scale and obtain nearly horizontal refractions from the upper mantle. Processing of gravity data was done at UiO and included correction of relative gravity meters readings using measurements at reference points in Tromsø and Longyearbyen, subtraction of normal gravity field computed for the WGS84 model, and Eötvös correction. The instrument drift was checked by gravity measurements in the port in Tromsø before departure and upon arrival using marine- and land gravimeters, and the drift was within 1 mGal. A Butterworth low-pass filter with cutoff wavelength of 5 km and the order of eight was applied to the gravity data. Comparison of the obtained free-air gravity anomaly with a regional dataset (ArcGP grid, Kenyon et al., 2008) shows a good match, however our measurements have a significantly better resolution.

3.3. Travel time modeling using Rayinvr

In order to map the crustal and upper mantle structure along the profile, a P-wave velocity model has been created using travel times recorded on the OBS hydrophone and vertical geophone components. The modeling was done using Rayinvr, a ray-tracing forward/inversion software developed by Zelt and Smith (1992). It allows an iterative approach based on trial and error until a reasonable fit between interpreted and calculated travel time curves is achieved. Following the forward modeling, inversion is performed layer by layer separately on velocity- and depth nodes. The inversion is useful for finding solutions in areas with complex geology and to derive resolution statistics.

Velocity models based exclusively on travel times recorded on widely spaced OBSs are non-unique and dependent on ray coverage, but additional constraints can be obtained from including other types of data. Information from MCS data and gravity data has thus been included to supplement the velocity model. The OBS profile is shot along an existing MCS profile, IKU-H (Fig. 1), and published interpretations of this line from Gudlaugsson et al. (1987) and Ritzmann and Faleide (2007) (Fig. 12) was used in the initial model building. Water depths were taken from the echo sounder data and the water layer was given a velocity of 1.48 km/s, a typical velocity for arctic seas (Grad et al., 2011). The geometry and velocity of the water layer was fixed during the modeling. A top-down strategy was used, starting with arrivals from the sedimentary section. The Rayinvr code allows for ray tracing of refracted-, reflected- and head waves. The goal is to obtain a velocity model that minimizes the travel time residuals (difference between picked and calculated arrivals) and where rays can be traced for as many picks as possible (Zelt and Forsyth, 1994). Arrivals on each of the individual OBS records are interpreted and used in the modeling. Data and model examples are show in Figs. 3–7, OBS 229, 226, 224, 214 and 212 are chosen because these records generally have a good data quality and illustrates the main features of the velocity model. Phase names used in the figures are listed in Table 1. During the interpretation each pick is given an uncertainty in time, often assigned to ± one typical cycle width of the phase (Breivik et al., 2003), and the goodness of fit can be estimated using a chi-squared (χ^2) criterion (e.g. Zelt and Forsyth, 1994). Typical uncertainties for the best arrivals are estimated to ±50 ms. Most Moho arrivals are given an uncertainty of ±90 ms if they are strong and clear, larger if they are weak. During the modeling an effort was made to obtain a χ^2 value of 1, which means that the travel time residual is equal to the pick uncertainty. A lower χ^2 value indicates overfitting (travel time residuals are less that the uncertainty of the picks), while a value larger than 1 imply that the residuals are higher that the pick uncertainty.

4. Results

4.1. P-wave travel time modeling

The final P-wave velocity model is divided into thirteen layers (Fig. 8). Some layers have similar velocities, but different velocity gradient. The quality of the data is generally good, however OBS 201, 221, 232 and 236 did not provide any useful data. The hydrophone component gave the best data for most of the stations, but on seven stations the vertical geophone component provided better data. The water layer (layer 1) is modeled with a constant velocity of 1.48 km/s and the water depth varies between 40 and 400 m along the profile. The youngest sedimentary rocks (layer 2), identified from MCS data tied to nearby wells, are Cretaceous in age (e.g. Faleide et al., 1984). Layer 2 has an average velocity of about 3.5 km/s and is thickest (1500 m) in the southeastern part of the profile within the Nordkapp Basin, and pinches out towards the northwest. In the NW end of the profile the velocities are higher, around 4.0 km/s just below the seafloor (layer 3). Based in interpretations of IKU-H (Gudlaugsson et al., 1987) the age of this sequence is expected to be Triassic.

A high-velocity layer is observed at a depth of 2 km on OBS 223-227 (layer 4). A velocity of 6 km/s gives a good fit between observed and calculated travel time however, shallow high velocities made it difficult to trace rays in the sedimentary section beneath layer 4. The velocity was therefore reduced from 6.0 km/s to 5.7–5.8 km/s, which gives a poorer fit but allowed more rays to be traced in the deeper layers. Layer 4 is approximately 200 m thick and 80 km long. Early Cretaceous magmatism has previously been reported in the area (Grogan et al., 2000; Breivik et al., 2002, 2003; Polteau et al., 2016) and the shallow high velocity layer is interpreted as a magmatic sill. Refractions from layer 6 require quite high velocities (5.8–5.9 km/s) Modeling of OBS 223 and 224 (Fig. 5) indicate velocity inversions in the sedimentary section and a low velocity layer (layer 5) had to be introduced beneath the sill in order to model refractions in layer 6. Layer 6 has lateral velocity variations that may represent change in lithology.

OBS 202, 203 and 204 are located in the Nordkapp Basin where salt diapirs (layer 7) rise to the seabed. At OBS 203 and 204 high-velocity arrivals are observed close to the seabed. MCS data (Grimstad, 2016) were used to constrain the geometry of the salt and the sedimentary layering in the Nordkapp Basin, and two strong reflections were interpreted as near Base Cretaceous Unconformity (BCU) and near Top Permian, respectively. The modeling is very sensitive to geometry, and the steep flanks of the salt make it difficult to trace rays through it. No refractions have been modeled in the salt; however several Moho reflections pass through it e.g. on OBS 212 (Fig. 7). Based on these arrivals the salt diapirs were modeled with a velocity of 5.0 km/s. Due to complex geometry and limited data quality no rays where traced at all for OBS 202 and 203. Velocity measurements from the sedimentary section just above top basement (layer 8) show a velocity of 5.8–5.9 km/s. A low contrast in seismic impedance between the sedimentary section and top of the crystalline basement results in weak or absent arrivals from this interface, making the interpretation uncertain. Some good basement refractions (P_g) have been recorded, mainly on OBS 214, 215, 218, 220, 226 and 227, constraining the velocity at top basement in the middle of the profile to 6.2 km/s. OBS 226 (Fig. 4) shows one of the strongest top basement arrivals as a refraction for larger offsets and a reflection for shorter offsets. OBS 226 also has some strong reflections from within the crystalline crust. Top basement is shallowest in the central parts of the model (7–8 km) and deepens to about 10 km beneath the Sørkapp

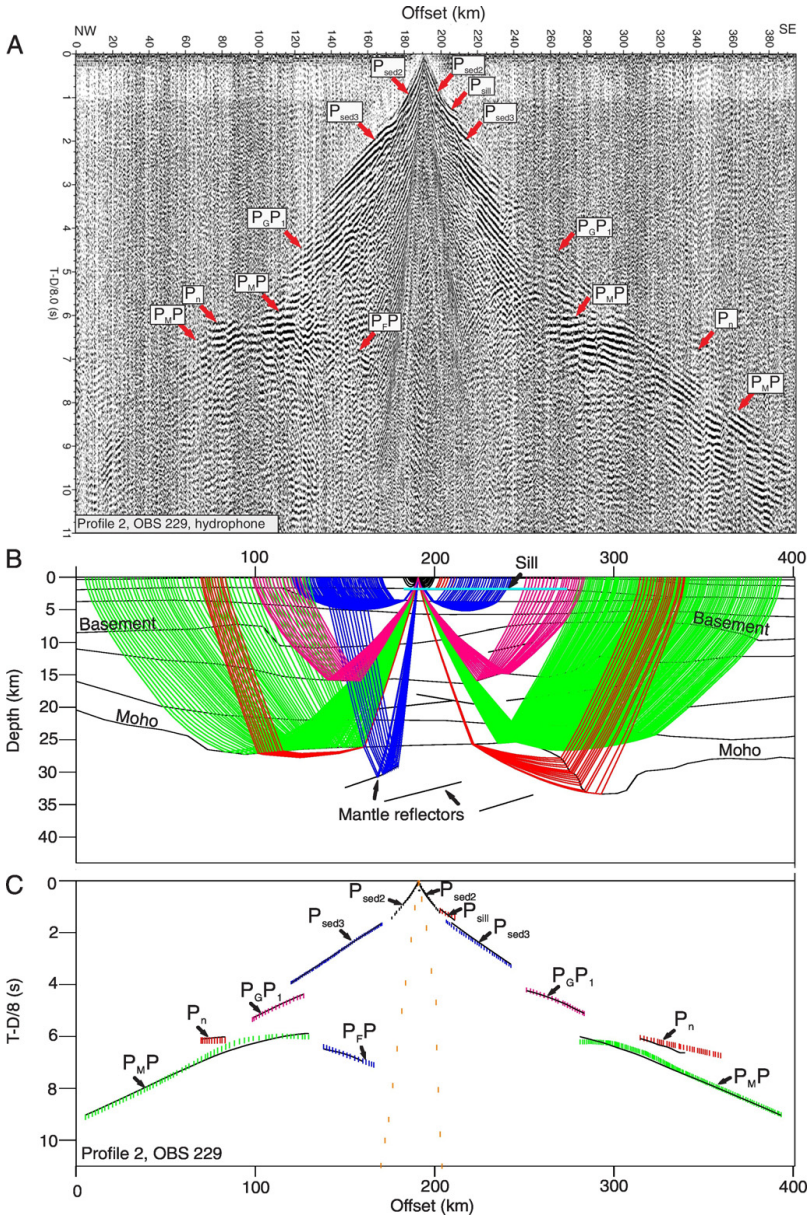

Fig. 3. A: Seismic data from OBS 229, Profile 2, hydrophone component (*BP-filter* (4-16 Hz), *spiking decon. and AGC applied*). Phase codes are listed in Table 1. B: Ray-paths through velocity layer model for OBS 229. C: Interpreted (vertical bars) and calculated travel-time curves.

Basin in the NW, and 12 km Nordkapp Basin in the SE (Fig. 8). Primarily based on the move-out of Moho reflections a velocity of 6.4–6.5 km/s has been modeled at base of the crust in the western part of the profile, while it increases to 6.7 km/s and 6.6 km/s in central and eastern parts, respectively. Many intra crustal reflections, sometimes of high amplitude, were identified. These events seem to originate from two levels, and the basement has therefore been divided into three layers (layer 9, 11 and 12). Several reflective events did not fit this layering and floating reflectors were therefore introduced. Layer 10 is a high velocity (6.9 km/s) layer at a depth of about 11 km. It has a limited extent and can only be seen on OBS 214 (Fig. 6). It may be interpreted as an intra-crustal sill intrusion.

OBS 229 offers a lot of information at offsets up to 190 km (Fig. 3). Clear refractions give velocities of 5.8–5.9 km/s in the sedimentary sequence (layer 6). The record shows a very strong Moho reflection and the move-out of this event is used to constrain the average velocity in

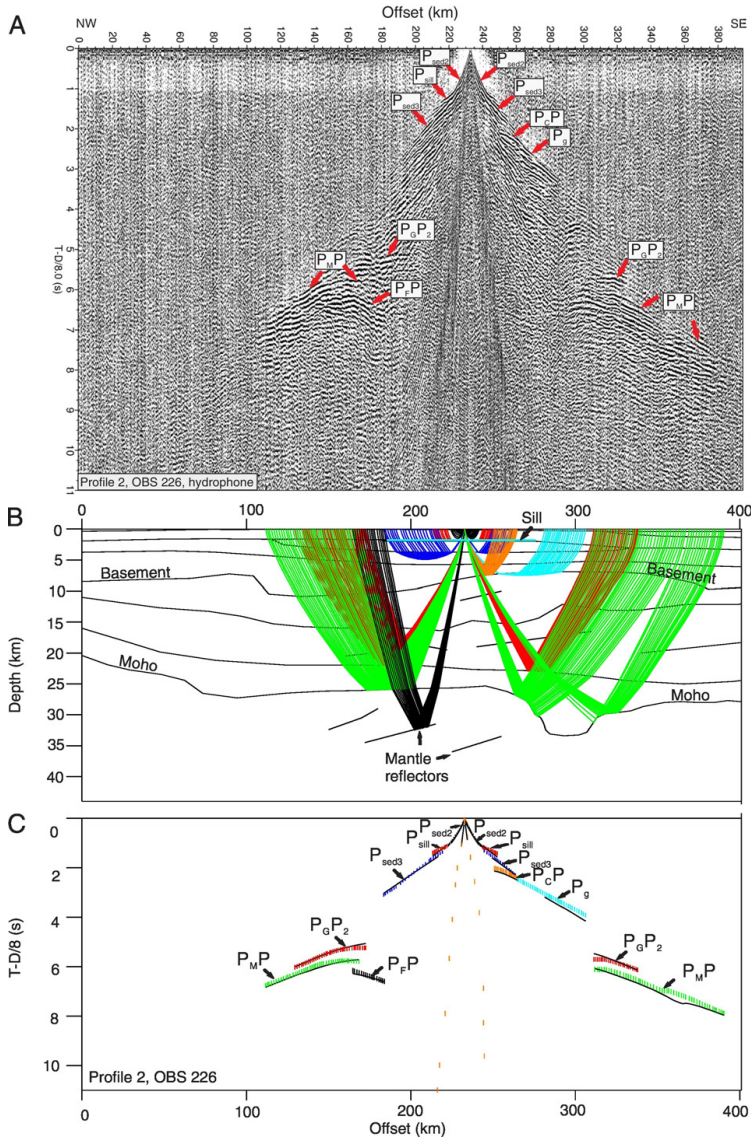

Fig. 4. A: Seismic data from OBS 226, Profile 2, hydrophone component (*BP-filter* (4–16 Hz), *spiking decon. and AGC applied*). Phase codes are listed in Table 1. B: Ray-paths through velocity layer model for OBS 226. C: Interpreted (vertical bars) and calculated travel-time curves.

the crust. A weak refraction from the upper mantle (P_n) is also recorded. Below the Moho there are some relatively strong reflections (P_FP) that seems to originate from within the top 10–15 km of the mantle. This upper mantle reflectivity appears to dip to the west-northwest, however they are not constrained by reversed observations and could have other origins.

Between 260 km and 300 km in the model (Fig. 8) Moho deepens by 6 km (from 27 km to 33 km) over a distance of 40 km. This is recorded particularly well on OBS 224 (Fig. 5), where the P_MP phase is recorded at about 6 s (reduced travel time) on the left side and about 7 s (reduced travel time) on the right side. Around 310 km (model distance) the Moho shallows to 28 km creating a "root structure" in the lower crust. This feature has been recorded consistently on neighboring OBSs. Another increase in Moho depth is observed on OBS 214 (Fig. 6) at 400 km along the profile. OBS 212 (Fig. 7) shows strong Moho reflections and a weak P_n phase, but there is limited information from within the crystalline crust. Some intra crustal reflections do appear when filtering away the highest frequencies. Refractions from the upper mantle (layer 13) recorded on OBS 211, 212, 214, 218, 220 and 223 fit well with a velocity of 8.0 km/s in the upper mantle.

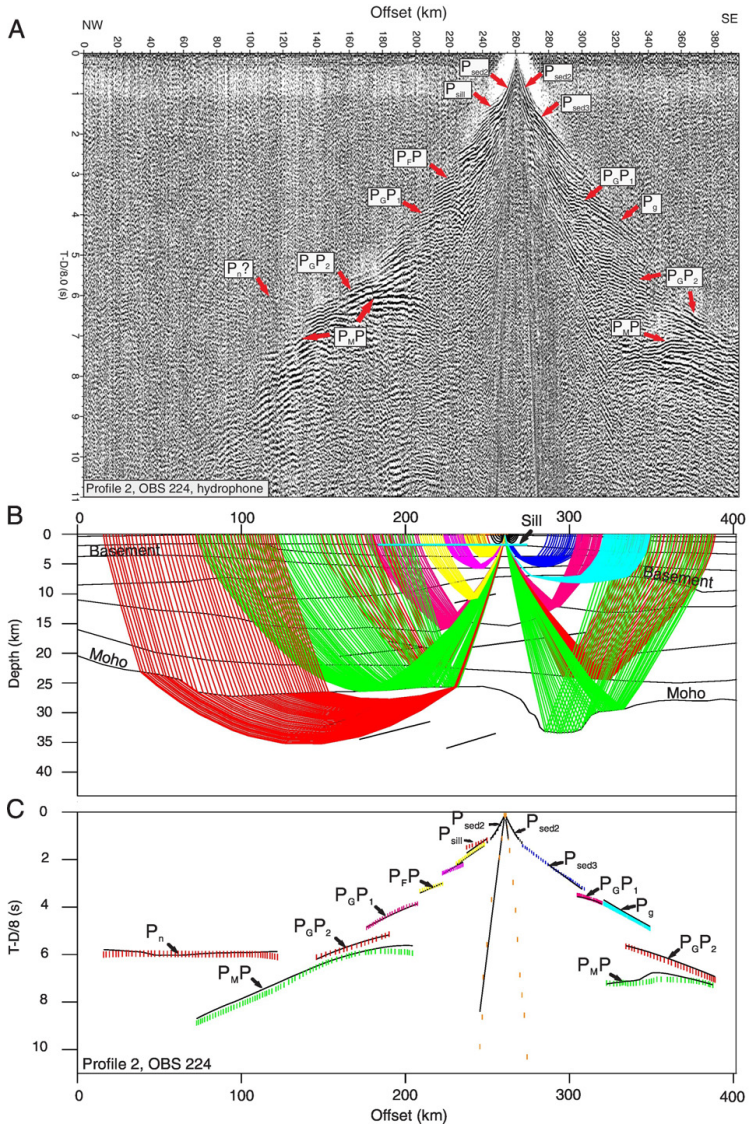

Fig. 5. A: Seismic data from OBS 224, Profile 2, hydrophone component (*BP-filter* (4–16 Hz), *spiking decon. and AGC applied*). Phase codes are listed in Table 1. B: Ray-paths through velocity layer model for OBS 224. C: Interpreted (vertical bars) and calculated travel-time curves.

4.2. Velocity model assessment

An assessment of the velocity model is done in order to evaluate how well the different parts of the model are constrained. The normalized $\chi^2$and RMS travel time residuals for the modeled phases are presented in Table 2, and ray hits for the final velocity model are shown in Fig. 9a. Most of the phases have a χ^2 value close to 1. Generally, ray coverage is best in the central parts of the profile, and the model is best constrained between 100 km and 530 km. Ray coverage is limited at both ends of the profile making these areas poorly resolved. Sedimentary layers 2, 3 and 6 is well covered with refracted waves and the velocity here are fairly well constrained. The shallow sill intrusion (layer 4) is not covered by many rays, but clear head waves have been modeled from this layer on OBS 229 and OBS 227-223. Clear refractions in the NW constrain the velocity at the top of layer 8, but the velocity structure is not well resolved in the SE part of the model.

The inversion tool in Rayinvr is used to obtain a resolution matrix in order to estimate how well the individual velocity nodes are constrained (Fig. 9b). Velocity nodes were inverted layer by layer using only refracted arrivals (node spacing 15–50 km), while keeping the geometry fixed. Values range from 0 to 1, with values from 0.5 and up indicating a fairly well resolved parameter (Zelt

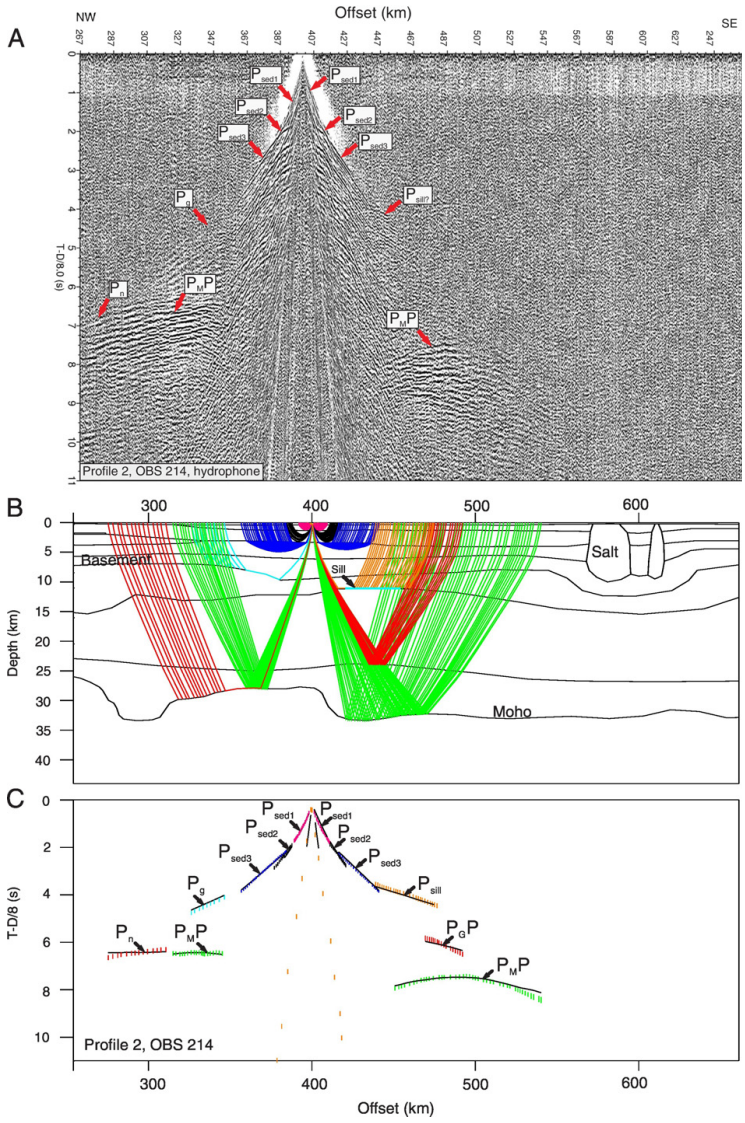

Fig. 6. A: Seismic data from OBS 214, Profile 2, hydrophone component (*BP-filter* (4–16 Hz), *spiking decon. and AGC applied*). Phase codes are listed in Table 1. B: Ray-paths through velocity layer model for OBS 214. C: Interpreted (vertical bars) and calculated travel-time curves.

and Smith, 1992). The depth node resolution was estimated for Moho (node spacing 10–30 km), while keeping the velocity fixed using both reflections and refractions. Larger circles around the depth nodes in Fig. 9b indicate better resolution.

The top of the crystalline crust is best constrained in the central parts of the model. In the NW end of the profile no top basement refractions have been recorded and the interpretation is based on reflections only. No direct velocity control was obtained from within the lower crust (layer 11 and 12); however the move-out of clear Moho reflections, recorded on almost all stations, gives the average velocity in the crust throughout the model, with the apparent velocity at maximum offset (50–200 km) approaching the velocity in the lowermost crust. Moho is constrained by both reflected and refracted arrivals. However, the poor control on velocity structure in the lower crust makes the Moho depth somewhat uncertain, particularly in the southern 100 km of the model. Fig. 9b indicates a poor depth node resolution in the crustal root area. The ray hit is limited due to the complex geometry, however clear PmP arrivals from OBS 226-223 and OBS 218 have been modeled here, suggesting that this feature is real. Some refractions from the upper mantle have been modeled, but the velocity structure here is not well constrained.

4.3. Gravity modeling

The ray-coverage (Fig. 9a) is controlled by the acquisition geometry and P-wave velocities. Gravity data have a different sampling and have

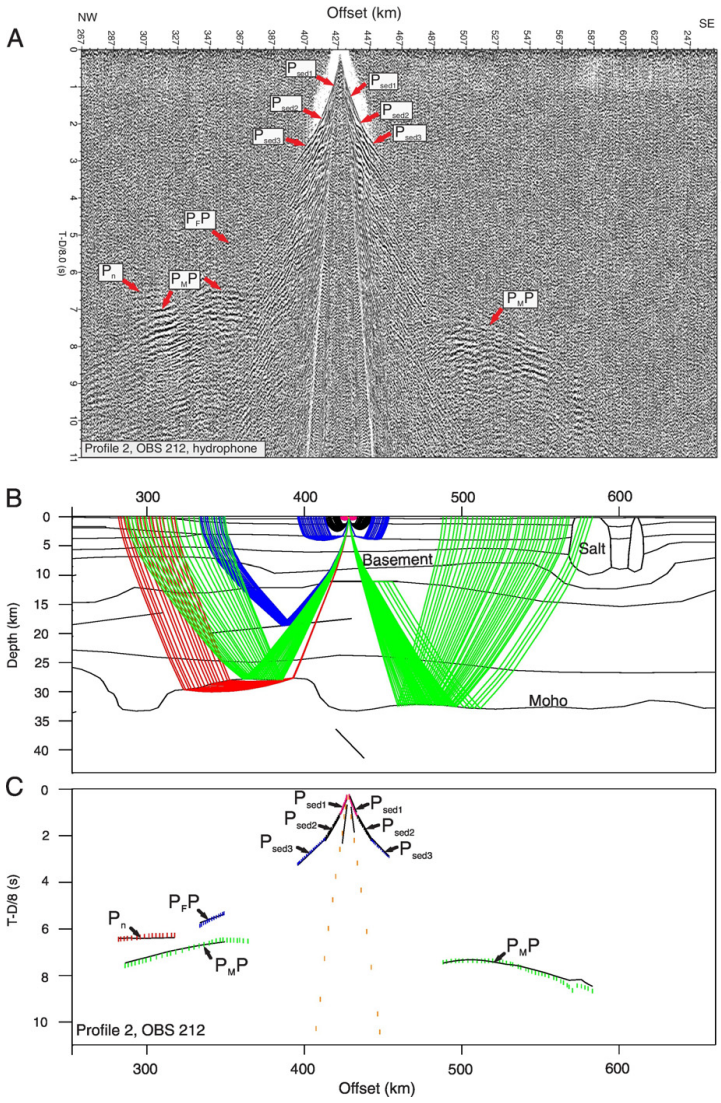

Fig. 7. A: Seismic data from OBS 212, Profile 2, hydrophone component (*BP-filter* (4–16 Hz), *spiking decon. and AGC applied*). Phase codes are listed in Table 1. B: Ray-paths through velocity layer model for OBS 212. C: Interpreted (vertical bars) and calculated travel-time curves.

the potential to add information to the model. A two-dimensional gravity model was made along the profile using the Oasis montaj GM-SYS Profile Modeling software. The gravity profile used in the modeling was recorded together with the OBS data and the observed gravity anomalies vary between −56 and 56 mGal. The strong positive gravity anomaly observed at the NW end of the profile is associated with the continent-ocean transition (COT) located a few km west of our profile, and has also been modeled by Breivik et al. (2003). There is also a positive gravity anomaly over the Gardarbanken High and a negative gravity anomaly due to the salt diapirs in the Nordkapp Basin. The velocity model was converted to a gravity model keeping the geometry of the layers. The average velocity in each layer was used to estimate initial density from an empirical velocity-density relationship (Ludwig et al., 1970; Barton, 1986). The model was extended 30,000 km in each direction to avoid edge effects. The results of the gravity modeling are presented in Fig. 10. The sedimentary section has been divided into three layers with densities of 2400 kg/m^3, 2620 kg/m^3 and 2740 kg/m^3. Additionally, the zone of increased velocities (part of layer 6, Fig. 8) above Gardarbanken High were modeled with a density of 2700 kg/m^3. Consistent with the velocity model, the crystalline crust have been divided into an upper, middle and lower layer and given densities based on the average velocity in each block, with values ranging from 2800 kg/m^3 to 2910 kg/m^3. These values are comparable to other models in the area, e.g. Marello et al. (2010) who used densities from 2710 to 2780 kg/m^3 and 2940 kg/m^3 for the upper and lower crust, respectively, and Klitzke et al. (2016) who used 2660–2800 kg/m^3 and

Table 1
List of abbreviations used for seismic events.

Phase	Code
P-wave refraction from sedimentary section 1	P_{sed1}
P-wave refraction from sedimentary section 2	P_{sed2}
P-wave refraction from sedimentary section 3	P_{sed3}
P-wave refraction at igneous sills	P_{sill}
P-wave refraction top basement	P_g
P-wave reflection top basement	P_CP
P-wave reflection from within crystalline crust 1	P_GP_1
P-wave reflection from within crystalline crust 2	P_GP_2
P-wave refraction from top mantle	P_n
P-wave reflection from Moho	P_MP
P-wave reflection from floating reflectors	P_FP

Table 2
Velocity model statistics for major refracted and reflected phases. P_GP_1 and P_GP_2 are reflections from upper and lower crustal layers. Total values include reflections that have not been listed.

Phase	Number of picks	T_{RMS} (ms)	Normalized chi-squared
P_{sed1}	337	111	1.988
P_{sed2}	656	72	1.332
P_{sed3}	1173	62	0.878
P_{sill}	63	87	1.565
P_g	343	94	1.165
P_CP	62	112	1.425
P_GP_1	181	65	0.597
P_GP_2	214	83	0.770
P_n	343	94	1.165
P_MP	1613	128	1.598
Total	5470	97	1.231

2977–3025 kg/m^3 for the upper and lower crust, respectively. The lateral increase in velocity eastwards is modeled as increased densities, dividing the crust into blocks. The data from Ludwig et al. (1970) show a considerable scatter in the velocity-density relationship, and a variation of ± 200 kg/m^3 is possible. During the modeling, the initial densities were not adjusted more than ± 30 kg/m^3. The lithosphere-asthenosphere boundary (LAB) is based surface wave tomography for the Barents Sea (Levshin et al., 2007) as applied by Klitzke et al. (2016). In accordance with the recent model of Klitzke et al. (2016), densities of 3330 and 3180 kg/m^3 have been used for the upper mantle lithosphere and asthenosphere, respectively.

Dividing the crust into even more block or adjusting the initial densities more gave a slightly better fit with the observed gravity field. However, in order to keep the model as simple as possible and without too many modifications, an error of 5.416 mGal is considered an acceptable fit between the observed and calculated gravity field. An attempt was also made to adjust the LAB, while keeping the crust homogenous, but this resulted in a very unrealistic topography of the LAB. The source of the anomaly above Gardarbanken High can lie in the sedimentary section or the crystalline crust (or both). The observed gravity can also be reproduced by introducing a block of increased density (3370 kg/m^3) in the upper mantle.

5. Discussion

5.1. Crustal structure

Velocities just below the seafloor vary from 3.4 km/s in the southeast to 4.0 km/s in the northwest. High velocities in the shallow sedimentary

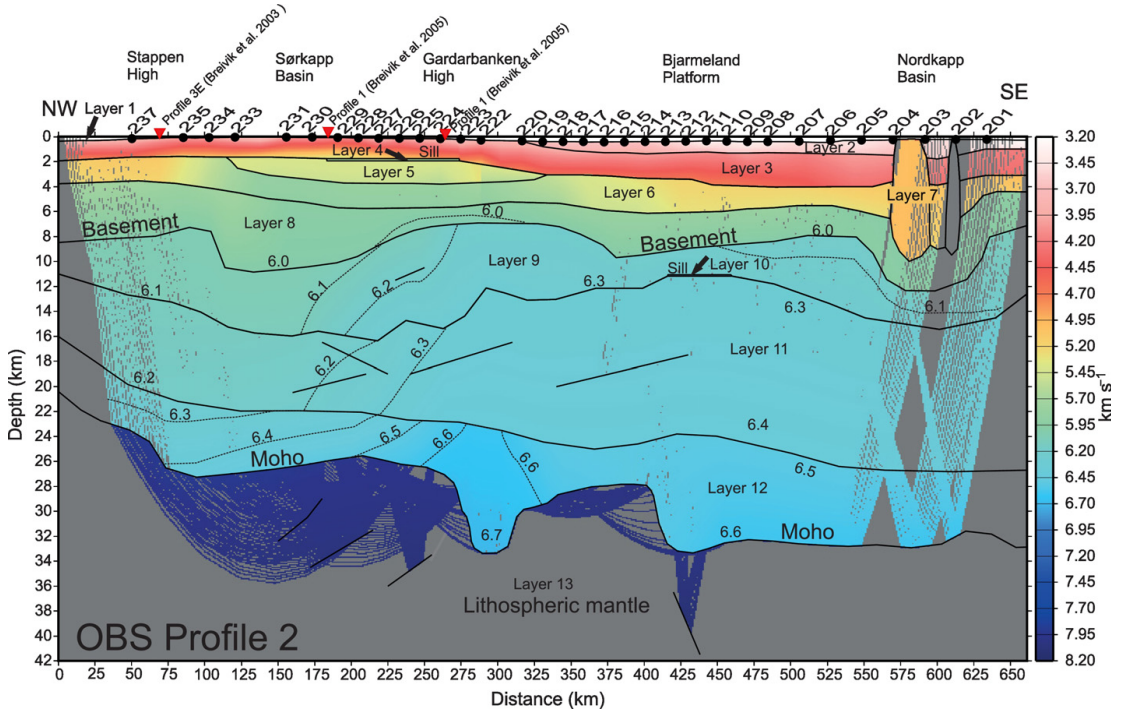

Fig. 8. P-wave velocity model of Profile 2 with layers numbered 1–13. Velocities from 6.0 to 6.6 km/s are contoured and annotated. Gray areas are not covered by ray-paths and are unconstrained. The location of crossing profiles is indicated by red triangles.

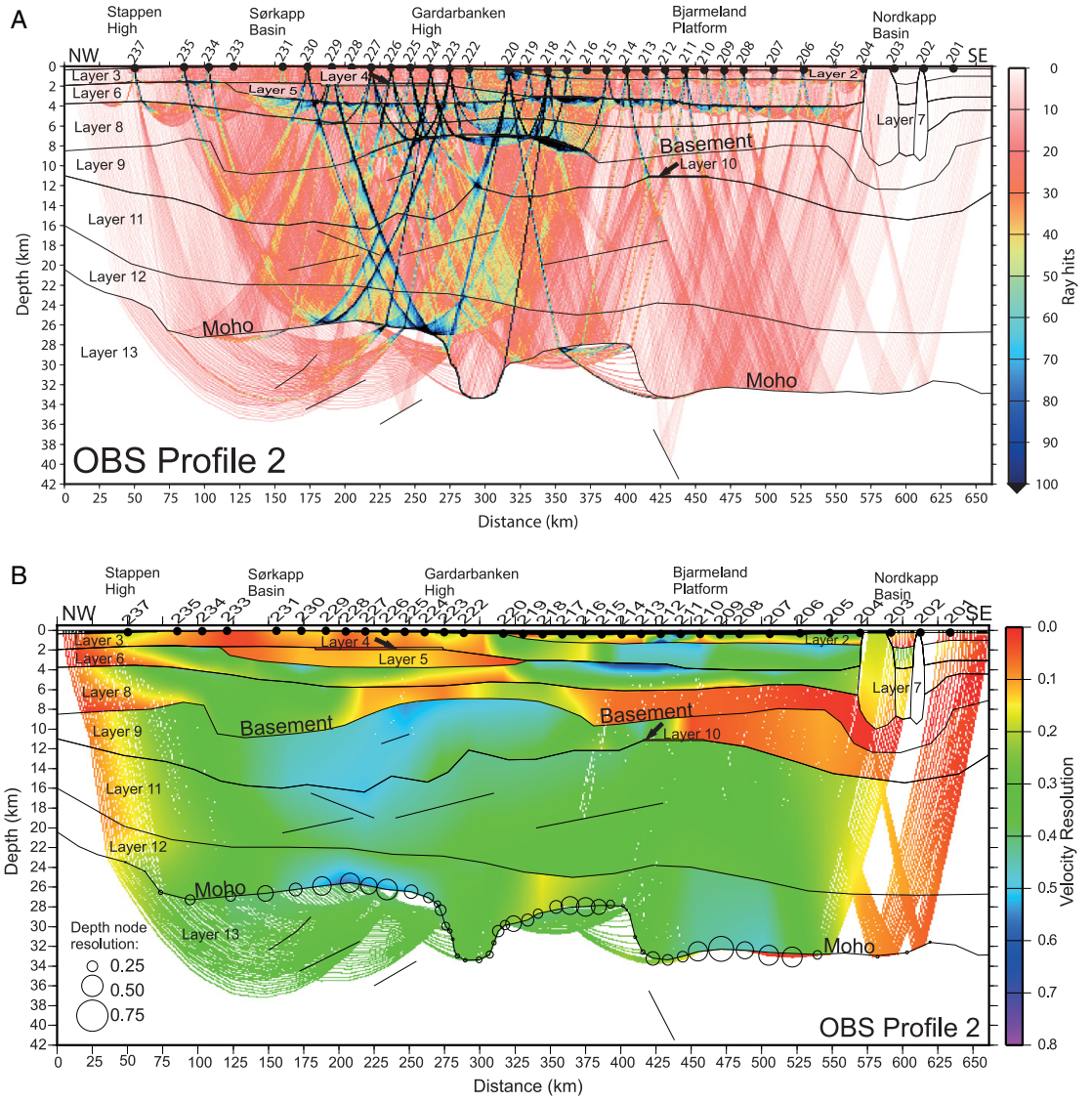

Fig. 9. A: Gridded ray coverage of the velocity model. The binning is 2.5 km horizontally and 0.25 km with depth. B: Resolution parameters of the velocity model. The velocity node resolution is shown by the color scale while the Moho depth resolution is given by the size of the circles, the larger the better constrained.

section are attributed to Late Cenozoic uplift and erosion (Eidvin et al., 1993; Dimakis et al., 1998; Grogan et al., 1999; Ohm et al., 2008; Henriksen et al., 2011b). Erosion has removed up to 3200 m from the sedimentary section in the northwestern end of the profile and about 1600 m in the southeastern end (e.g. Dimakis et al., 1998; Henriksen et al., 2011b). Increased velocities in the northwest end of the profile correlate with increased net erosion in the Stappen High area. The deepest basement can be found under the Sørkapp- and Nordkapp Basins (Fig. 8) where the depths reach 10 km and 12 km, respectively. The Sørkapp Basin is defined at Permian and Triassic levels (Gabrielsen et al., 1990; Grogan et al., 1999) (Fig. 1). The main basin subsidence occurred in the Triassic, but reflection seismic data indicate that Palaeozoic carbonates is underlain by an older basin, possibly of Early Carboniferous and/or Devonian age (Gabrielsen et al., 1990). Gudlaugsson and Faleide (1994) and Breivik et al. (2003, 2005) identified a deep basin a few km northeast of our profile with basement depths reaching 14 km, coinciding with the Sørkapp Basin. This basin was constrained to the west and north, but not to the east and south. The basin modeled here could be the southwest continuation of that basin, were the southeastern flank is constrained by top basement refractions and the northwestern flank by top basement reflections on OBS 234 and IKU-H. The basin coincides well with the model of Klitzke et al. (2016), who also modeled basement depth around 10 km in this area. The Sørkapp Basin is often drawn as a slightly N—S

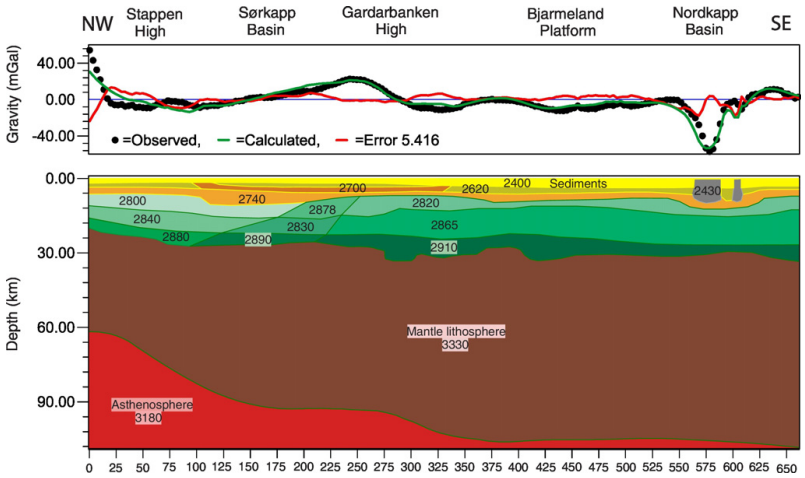

Fig. 10. Gravity model along Profile 2. Numbers on figure are densities in kg/m^3. Sedimentary rocks are shown in yellow and basement blocks in green.

elongated basin on structural maps (e.g. Gabrielsen et al., 1990; Faleide et al., 1993) however, Anell et al. (2014) suggested a NE-SW to E-W trend. Comparing our model with three older OBS profiles modeled by Breivik et al. (2002, 2005) (Figs. 1 and 11) we favor a NE-SW trend of the Sørkapp Basin, in accordance with previous interpretations of rift basins in southwestern Barents Sea (e.g. Gudlaugsson et al., 1998; Faleide et al., 2008). The outline of the Sørkapp Basin is drawn on Fig. 11. Its northwestern and southeastern boundary is fairly well

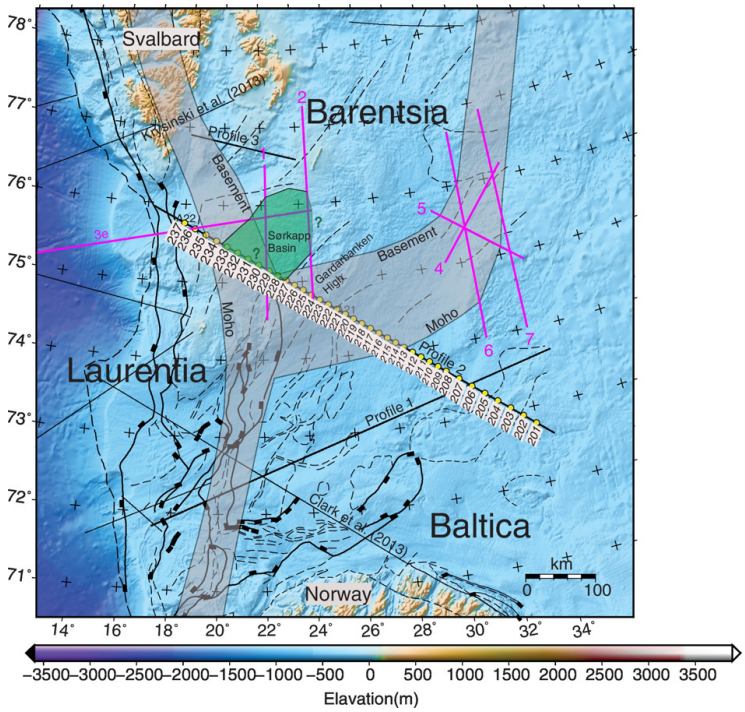

Fig. 11. Location of the modeled profile with OBS locations shown as yellow dots. The shaded gray area indicates the location of the proposed Caledonian suture zones. The map is based on a Caledonide model of Gudlaugsson et al. (1998) and OBS profiles (in pink) modeled by Breivik et al. (2002, 2003, 2005), Clark et al. (2013) and Krysinski et al. (2013). The edges of the gray area is where the suture zone cuts top basement and Moho. The Sørkapp Basin is outlined in green.

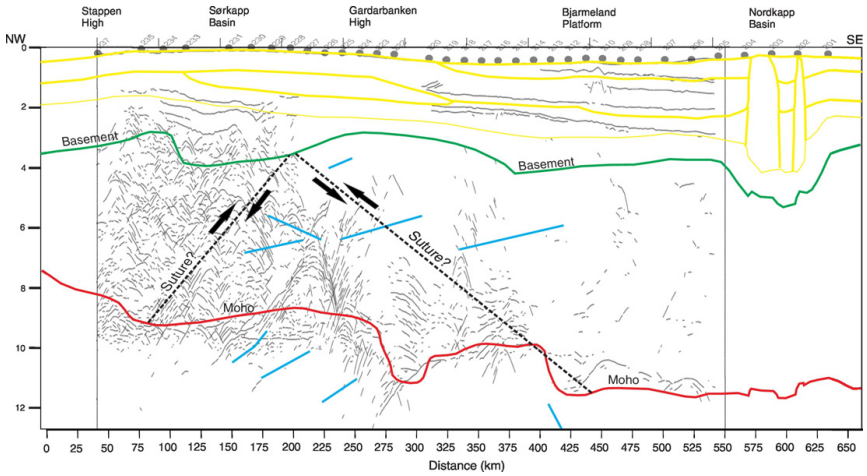

Fig. 12. Crustal structure from OBS data compared to linedrawing of the MCS line IKU-H. Colored and stippled lines are from the OBS data, floating reflectors are indicated in blue. The proposed Caledonian suture from Figs. 12 and 13 separates the reflective basement in the west from the more transparent basement in the east.
(Modified from Gudlaugsson et al. (1987) and Ritzmann and Faleide (2007).)

constrained by OBS data, whereas the continuation to the east and southwest is uncertain.

The modeled profile is shot along the deep seismic line IKU-H, and layer boundaries from the time-converted velocity model are overlain on interpretations of IKU-H in Fig. 12. There is a good fit between the OBS data and the MCS data in the sedimentary section (at 1.9 s) in the NW end of the profile, but the two datasets seem to have picked up slightly different reflections across the Bjarmeland Platform. Top of the crystalline crust is difficult to interpret from MCS data, especially in the eastern part. In the NW end the top of the chaotic reflective zone around 3 s could be interpreted as top of the crystalline crust, but from the OBS data it is interpreted to lie deeper under the Sørkapp Basin. Assuming the P-wave velocity model from the OBS data is correct, the top of the chaotic reflective package could be interpreted as meta-sedimentary rocks overlying crystalline crust.

The Moho topography between 260 km and 340 km in the model is interpreted as a Caledonian "root structure". Similar structures associated with high velocities in the upper mantle (8.5 km/s) have been modeled in the Sentralbanken High region (Breivik et al., 2002) where high velocities and densities in the upper mantle were interpreted as eclogitized oceanic crust associated with a proto-Caledonian subduction zone, with the crustal root as a remnant of the continental collision. A crustal root structure has also been observed along the deep seismic line IKU-D (Fig. 1) south of Svalbard, and interpreted to be a proto-Caledonian subduction zone dipping to the west (Gudlaugsson and Faleide, 1994; Breivik et al., 2005). Farther southeast along the profile, around 400 km, another prominent increase in Moho depth has been modeled.

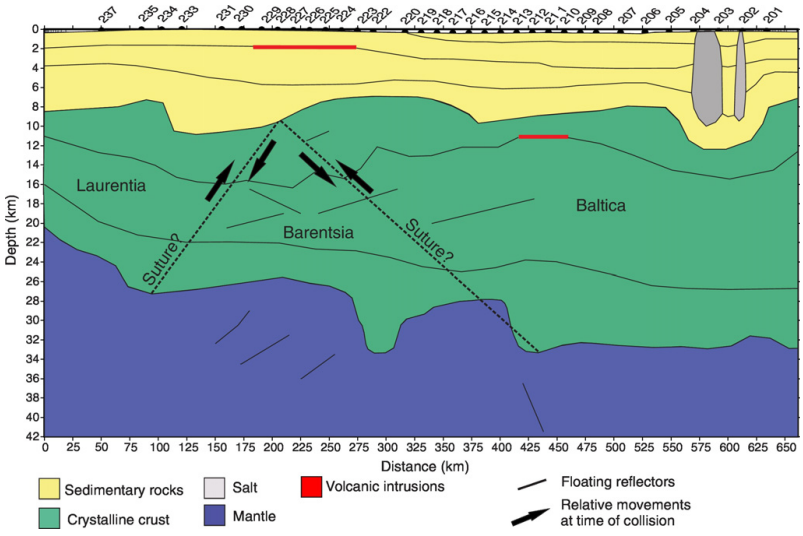

Fig. 13. Tectonic model of the modeled OBS profile.

This structure is most likely related to the boundary between two different basement domains (Figs. 12 and 13), but how it is linked to structures shallower in the crust is uncertain. There is generally a good correspondence in Moho depth between OBS data and IKU-H. In the western part of IKU-H the basement is very reflective down to about 10 s and the base of this reflective zone is interpreted as Moho. In the velocity model Moho is located 0.5–1.0 s shallower, but many floating reflectors have been modeled in the upper mantle, suggesting that the base of the reflective zone on IKU-H does not represent Moho, but rather a reflective zone in the upper mantle. Another explanation for the misfit could be that OBS data generally measure more horizontal and therefore higher velocities, resulting in a shallower Moho interpretation. Additionally, some of the dipping reflections on IKU-H could be diffractions (the line is not migrated, but a dip filter have been applied to remove some of the diffractions). On OBS 229 a weak arrival with an apparent P-wave velocity of 7.1 km/s has been modeled as a Pn phase. A good fit between observed and modeled travel times can be achieved by introducing as a high-velocity (7.1 km/s) layer in the lower crust. However, such a layer disrupts several strong PmP arrivals on OBS 223-229. Lacking support from other OBSs, it was considered more important to fit the strong PmP-arrivals, and a high-velocity layer in the lower crust was not included in the model.

5.2. Tectonic domains and comparison with nearby seismic profiles

The modeled profile crosses three older OBS profiles and velocities and densities at the cross points are listed in Table 3. In cross point 1 (Profile 3e from Breivik et al. (2003) and OBS 236, Fig. 1), the depth to crystalline crust is 8 km in both profiles. Cross point 2 and 3 is located in the central parts of the model (at OBS 224 and 229, respectively) and at the southern ends of Profile 1 and 2 from Breivik et al. (2005). The difference in modeled depth to crystalline crust is quite large at the cross points, between 3 and 4 km. However, the southern ends of Profile 1 and 2 is poorly constrained by seismic data and the basement depths are uncertain, and the interpretation from our study is therefore preferred. Breivik et al. (2003) has modeled a deeper Moho (29 km) compared to this study (26 km). A northwestward shallowing of the Moho was introduced in cross point 1 based on the positive gravity anomaly at the NW end and the COB located a few km west of the profile. This shallowing of Moho was also modeled by Breivik et al. (2003). Cross point 1 is at the northwestern edge of the model and is poorly constrained by seismic data, and no thermal effects of the adjacent young oceanic lithosphere were incorporated, so the old model should be the most reliable in this area.

The velocity model in Fig. 8 shows significantly lower basement velocities in the western (6.05–6.5 km/s) than the eastern part (6.2–6.7 km/s). This eastwards increase in velocity was also modeled by Breivik et al. (2003) farther north and could to be related to a possible suture between Laurentia in the west and Barentsia in the east (Figs. 11 and 13). Based on the velocity structure in the crystalline crust and the geometry of the upper mantle reflectivity (Fig. 8) our model supports the interpretation of Breivik et al. (2003) with a westward dipping suture between Laurentia and Barentsia. However, we propose that the Laurentia-Barentia suture is located about 50 km farther west than the suture proposed by Breivik et al. (2003), cutting top basement close to the location of OBS 228 (Figs. 11, 13). Primarily based on potential field data this suture has been traced northwards in Storfjorden and along the Billefjorden Fault Zone. This is supported by Agard et al. (2005) who documents a Caledonian subduction in western Spitsbergen and Krysinski et al. (2013) who modeled OBS profiles across Spitsbergen and Storfjorden (Fig. 11) and interpreted variations in crustal thickness, velocities and densities to represent the main Caledonian suture between Laurentia and Barentsia. The suture may also be traced further south, between the Bjørnøya Basin and the Loppa High (Clark et al., 2013, Fig. 11). No lateral velocity change can be observed across the Barentsia-Baltica suture from the modeled OBS data. However, the change in reflective character across this boundary, observed both from the OBS data (Fig. 9a) and vintage MCS data (Fig. 12), suggest that these two blocks consist of materials with different physical properties. An eastward decrease in reflectivity has also been observed further north along IKU-D, and has been proposed to represent a Caledonian suture zone separating Barentsia from Baltica (Gudlaugsson and Faleide, 1994). This interpretation is supported by modeled OBS data along the same line (Profile 3e, Fig. 1) (Breivik et al., 2003).

5.3. Tectonic model

Generally N-striking Caledonian basement with Laurentian affinities is exposed in the Svalbard Archipelago (Harland et al., 1997) and most of Svalbard's Caledonian terranes are considered to be the direct northerly continuation of the Caledonides of eastern Greenland (e.g. Higgins and Leslie, 2000). Caledonian migmatization is found as far east as Kvitøya (Gee, 2004) (Fig. 2), about 100 km east of Nordaustlandet, suggesting that a substantial part of the Barents Shelf is underlain by Caledonian basement and that Caledonian suture(s) must be located even farther to the east. Deep drilling on Franz Josef Land reached turbidites of Vendian age with folding proposed to be Caledonian (Dibner, 1998). Farther northeast, on Severnaya Zemlya, folding and thrusting of Devonian Old Red Sandstone has been related to late Caledonian deformation (Lorenz et al., 2007). No Caledonian deformation has been recorded in the island of Novaya Zemlya. A Caledonian suture through the Barents Sea between Kvitøya and western Franz Josef Land has been favored (Gee et al., 2006; Barrère et al., 2011). The Caledonian deformation front has been inferred to trend northeastwards between Franz Josef Land and Novaya Zemlya (Fig. 2).

Based on the orientation of basins and highs on the Barents Sea shelf (e.g. Nordkapp Basin, Hammerfest Basin, Loppa High, and Sentralbanken High) it has been proposed that the Caledonian suture follows this northeasterly trend in the Barents Sea (Doré, 1991; Gudlaugsson et al., 1998). Gudlaugsson et al. (1998) and Breivik et al. (2002) suggested that the Caledonian orogeny consists of two branches north of Norway, one along western Spitsbergen and one northeast through the Barents Sea. Torsvik et al. (2001) proposed that Svalbard acted as an independent crustal block in the early Palaeozoic, and probably collided with NE Greenland in Late Ordovician times, and subsequently colliding with Baltica during the Mid-Late Silurian. The model of Breivik et al. (2002) is in accordance with this interpretation, with the microcontinent "Barentsia" (not corresponding entirely to the islands of Svalbard)

Table 3
Profile 2 compared with three crossing seismic profiles. Velocities and densities listed are at the top and bottom of the given unit. The location of crossing profiles is shown on Figs. 1, 8 and 11.

	Crosspoint 1		Crosspoint 2		Crosspoint 3	
	Laurentia		Barentsia		Barentsia/Baltica	
	P3e	OBS 236	P1	OBS 229	P2	OBS 224
Sedimentary unit: Vp (km/s)	4.0–6.0	4.0–6.0	4.0–6.0	4.0–6.0	4.0–6.0	4.0–6.0
Sedimentary unit: δ (g/cm3)	2.46–2.69	2.40–2.75	2.40–2.75	2.40–2.75	2.40–2.75	2.40–2.75
Crystalline crust: Vp (km/s)	6.2–6.4	6.05–6.4	6.2–6.6	6.1–6.5	6.2–6.6	6.2–6.6
Crystalline crust: δ (g/cm3)	2.798	2.78–2.87	2.797	2.82–92	2.818	2.82–92

between Laurentia and Baltica. This scenario has also been supported by magnetic data (Marello et al., 2013), as Barentsia is distinguished from the rest of the Barents Sea shelf by its low-magnetic properties and large crustal thickness. Marello et al. (2013) agreed with the proposed location of the Barentsia-Baltica suture (Breivik et al., 2002) and extended it further north-northeastwards to the western Franz Josef Land. Breivik et al. (2002) proposed a Caledonian suture located under and following the trend of the Sentralbanken High, and interpreted the thickest parts of the crust to be created by a subduction zone dipping to the southeast, terminating in continent-continent collision. The central parts of the modeled profile lie in the southwestward continuation of the proposed suture trend, and a suture dipping to the southeast fits well with the observed change in reflective character and the deepening of Moho around 400 km (Fig. 12).The polarity of the suture can be discussed. A zone of westward dipping reflectivity in the lower crust along IKU-H has been interpreted by Gudlaugsson et al. (1987) as overthrusting eastwards. However, this zone is located so far to the west that is might be associated with the Svalbard Caledonides. Also the image along IKU-H is blurred by a lot of diffraction hyperbolas dipping in both directions, and it is very difficult to distinguish dip directions of faults or sutures from diffractions. Based on potential field data Marello et al. (2013) supports the possible location of the inferred suture but suggested a dip towards the northeast.

6. Summary and conclusions

We present a P-wave velocity model across the Arctic Caledonian basement province based on modeling of travel times recorded on 32 ocean bottom seismometer stations along an ~660 km long profile in the western Barents Sea. The geometry of the shallow sedimentary section is constrained by seismic reflection profiles. P-wave velocities in the sedimentary unit are generally higher in the northwestern part of the profile (4.2–5.2 km/s) than in the eastern (3.2–4.5 km/s), attributed to increased erosion towards Svalbard and the continental margin. Two zones of anomalously high velocities in the upper crust (6.0 km/s and 6.9 km/s) have been interpreted as magmatic sills, probably emplaced during the Early Cretaceous. Depth to basement is constrained to 7 km in the middle of the profile, increasing to 10 km and 12 km beneath the Sørkapp Basin and Nordkapp Basin, respectively. Combining the profile modeled here with previously published velocity models along nearby OBS profiles, we favor a NE-SW trend of the Sørkapp Basin. Local deepening of Moho (from 27 km to 33 km depth) creates “root structures” that can be linked to the Caledonian compressional deformation or a suture zone imprinted in the crust. A sharp increase in velocities in the crystalline basement (from 6.0–6.4 km/s in the northwest to 6.1–6.6 km/s in the southeast) has been interpreted in terms of two distinct tectonic terranes: Laurentia and Barentsia. We further infer a westward subduction of Barentsia beneath Laurentia based on the pattern of seismic velocities and geometry of mid-crustal reflectors. The eastwards decrease in reflectivity observed along a vintage multichannel seismic line (IKU-H) is supported by the new OBS data, and interpreted to represent the suture between Barentsia and Baltica. Our model supports the existence of a separate NE-SW trending Caledonian branch extending into the Barents Sea, linking up with the northerly trending Svalbard Caledonides, with Barentsia as an independent microcontinent between Laurentia and Baltica.

Acknowledgements

This work was supported by the Research Council of Norway FRINATEK program through BarPz project 234153. We would like to thank all the participating institutions and the crew onboard R/V Håkon Mosby. Ole Meyer, Stig Monsen and Patrice Bretel from the University of Bergen and Alexey Shulgin and Nina Lebedeva-Ivanova from the University of Oslo and Ann-Marie Vølsch, Jasmin Møgeltønder and Kathrin M. Lieser from GEOMAR are thanked for their contribution during the OBS acquisition. We also thank Alexey Shulgin for pre-processing parts of the OBS data. A.J. Breivik, J.I. Faleide and A. Minakov acknowledge support from the Research Council of Norway through its Centres of Excellence funding scheme, project number 223272. The modeling was done using Rayinvr provided by Dr. C. Zelt (Rice University, Houston). GMT (Wessel and Smith, 1998) has been used to generate several of the maps in this paper.

Appendix A. Supplementary data

Supplementary data to this article can be found online at http://dx.doi.org/10.1016/j.tecto.2017.04.022.

References

Agard, P., Labrousse, L., Elvevold, S., Lepvrier, C., 2005. Discovery of Paleozoic Fe-Mg carpholite in Motalafjella, Svalbard Caledonides: a milestone for subduction-zone gradients. Geology 33 (10):761–764. http://dx.doi.org/10.1130/G21693.1.

Anell, I., Braathen, A., Olaussen, S., 2014. Regional constraints of the Sørkapp Basin: a Carboniferous relic or a Cretaceous depression? Mar. Pet. Geol. 54:123–138. http://dx.doi.org/10.1016/j.marpetgeo.2014.02.023.

Barrère, C., Ebbing, J., Gernigon, L., 2009. Offshore prolongation of Caledonian structures and basement charaterisation in the western Barents Sea from geophysical modelling. Tectonophysics 470 (1–2), 71–88.

Barrère, C., Ebbing, J., Gernigon, L., 2011. 3-D density and magnetic crustal characterization of the southwestern Barents Shelf: implications for the offshore prolongation of the Norwegian Caledonides. Geophys. J. Int. 184 (3):1147–1166. http://dx.doi.org/10.1111/j.1365-246X.2010.04888.x.

Barton, P.J., 1986. The relationship between seismic velocity and density in the continental crust—a useful constraint? Geophys. J. R. Astron. Soc. 87:195–208. http://dx.doi.org/10.1111/j.1365-246X.1986.tb04553.x.

Bergh, S.G., Maher Jr., H.D., Braathen, A., 2011. Late Devonian transpressional tectonics in Spitsbergen, Svalbard, and implications for basement uplift of the Sørkapp-Hornsund High. J. Geol. Soc. Lond. 168:441–456. http://dx.doi.org/10.1144/0016-76492010-046.

Blinova, M., Faleide, J.I., Gabrielsen, R.H., Mjelde, R., 2013. Analysis of structural trends of sub-sea-floor strata in the Isfjorden area of the West Spitsbergen Fold-and-Thrust Belt based on multichannel seismic data. J. Geol. Soc. Lond. 170:657–668. http://dx.doi.org/10.1144/jgs2012-109.

Breivik, A.J., Faleide, J.I., Gudlaugsson, S.T., 1998. Southwestern Barents Sea margin: late Mesozoic sedimentary basins and crustal extension. Tectonophysics 293:21–44. http://dx.doi.org/10.1016/S0040-1951(98)00073-0.

Breivik, A.J., Verhoef, J., Faleide, J.I., 1999. Effect of thermal contrasts on gravity modeling at passive margins: results from the western Barents Sea. J. Geophys. Res. 104 (B7): 15293–15311. http://dx.doi.org/10.1029/1998JB900022.

Breivik, A.J., Mjelde, R., Grogan, P., Shimamura, H., Murai, Y., Nishimura, Y., Kuwano, A., 2002. A possible Caledonide arm through the Barents Sea imaged by OBS data. Tectonophysics 355:67–97. http://dx.doi.org/10.1016/S0040-1951(02)00135-X.

Breivik, A.J., Mjelde, R., Grogan, P., Shimamura, H., Murai, Y., Nishimura, Y., 2003. Crustal structure and transform margin development south of Svalbard based on ocean bottom seismometer data. Tectonophysics 369:37–70. http://dx.doi.org/10.1016/S0040-1951(03)00131-8.

Breivik, A.J., Mjelde, R., Grogan, P., Shimamura, H., Murai, Y., Nishimura, Y., 2005. Caledonide development offshore-onshore Svalbard based on ocean bottom seismometer, conventional seismic, and potential field data. Tectonophysics 401: 79–117. http://dx.doi.org/10.1016/j.tecto.2005.03.009.

Churkin Jr., M., Soleimani, G., Carter, C., Robinson, R., 1981. Geology of the Soviet Arctic: Kola Peninsula to Lena river. In: Nairn, A.E.M., Churkin, M.J., Stehli, F.G. (Eds.), The Ocean Basins and Margins. The Arctic Ocean 5, pp. 331–375.

Clark, S.A., Faleide, J.I., Hauser, J., Ritzmann, O., Mjelde, R., Ebbing, J., Thybo, H., Flüh, E., 2013. Stochastic velocity inversion of seismic reflection/refraction traveltime data for rift structure of the southwest Barents Sea. Tectonophysics 593:135–150. http://dx.doi.org/10.1016/j.tecto.2013.02.033.

Cocks, L.R.M., Torsvik, T.H., 2011. The Palaeozoic geography of Laurentia and western Laurussia: a stable craton with mobile margins. Earth Sci. Rev. 106 (1–2):1–51. http://dx.doi.org/10.1016/j.earscirev.2011.01.007.

Dengo, C.A., Røssland, K.G., 1992. Extensional tectonic history of the western Barents Sea. In: Larsen, R.M., Brekke, H., Larsen, B.T., Talleraas, E. (Eds.), Structural and Tectonic Modelling and Its Applications to Petroleum Geology. 1. Norwegian Petroleum Society Special Publication, Trondheim, pp. 91–107.

Dibner, V.D., 1998. The geology of Franz Joseph Land—an introduction. In: Solheim, A., Musatov, E., Heintz, N. (Eds.), Geological Aspects of Franz Joseph Land and the Northernmost Barents Sea. 151. Norsk Polarinstitutt Meddelelser, pp. 24–46.

Dimakis, P., Braathen, B.I., Faleide, J.I., Elverhøi, A., Gudlaugsson, S.T., 1998. Cenozoic erosion and the preglacial uplift of the Svalbard-Barents Sea region. Tectonophysics 300: 311–327. http://dx.doi.org/10.1016/S0040-1951(98)00245-5.

Doré, A.G., 1991. The structural foundation and evolution of Mesozoic seaways between Europe and the Arctic. Palaeogeogr. Palaeoclimatol. Palaeoecol. 87:441–492. http://dx.doi.org/10.1016/0031-0182(91)90144-G.

Eidvin, T., Jansen, E., Riis, F., 1993. Chronology of Tertiary fan deposits off the western Barents Sea: implications for the uplift and erosion history of the Barents shelf. Mar. Geol. 112:109–131. http://dx.doi.org/10.1016/0025-3227(93)90164-Q.

Faleide, J.I., Gudlaugsson, S.T., Jacquart, G., 1984. Evolution of the western Barents Sea. Mar. Pet. Geol. 1:123–150. http://dx.doi.org/10.1016/0264-8172(84)90082-5.
Faleide, J.I., Vågnes, E., Gudlaugsson, S.T., 1993. Late Mesozoic-Cenozoic evolution of the south-western Barents Sea in a regional rift-shear tectonic setting. Mar. Pet. Geol. 10:186–214. http://dx.doi.org/10.1016/0264-8172(93)90104-Z.
Faleide, J.I., Tsikalas, F., Breivik, A.J., Mjelde, R., Ritzmann, O., Engen, O., Wilson, J., Eldholm, O., 2008. Structure and evolution of the continental margin off Norway and Barents Sea. Episodes 31 (1), 82–91.
Gabrielsen, R.H., 1984. Long-lived fault zones and their influence on the tectonic development of the southwestern Barents Sea. J. Geol. Soc. Lond. 141:651–662. http://dx.doi.org/10.1144/gsjgs.141.4.0651.
Gabrielsen, R.H., Færseth, R.B., Jensen, L., Kalheim, J.E., Riis, F., 1990. Structural elements of the Norwegian continental shelf: part 1. The Barents Sea Region. NDP Bull. Nor. Petrol. Dir. 6 (Stavanger, Norway).
Gac, S., Huismans, R.S., Podladchikov, Y.Y., Faleide, J.I., 2012. On the origin of the ultradeep East Barents Sea basin. J. Geophys. Res. 117, B04401. http://dx.doi.org/10.1029/2011JB008533.
Gee, D.G., 2004. The Barentsian Caledonides: death of the High Arctic Barents Craton. In: Smelror, M., Bugge, T. (Eds.), Arctic Geology, Hydrocarbon Resources and Environmental Challenges. NGF Abstracts and Proceedings 2, pp. 48–49.
Gee, D.G., Teben'kov, A.M., 2004. Svalbard: a fragment of the Laurentian margin. In: Gee, D.G., Pease, V.L. (Eds.), The Neoproterozoic Timanide Orogen of Eastern Baltica. Memoirs Geological Society of London 30, pp. 191–206.
Gee, D.G., Bogolepova, O.K., Lorenz, H., 2006. The Timanide, Caledonide and Uralide orogens in the Eurasian high Arctic, and relationships to the palaeo-continents Laurentia, Baltica and Siberia. In: Gee, D.G., Stephenson, R.A. (Eds.), European Lithosphere Dynamics. Memoirs Geological Society of London 32, pp. 507–520.
Gee, D.G., Fossen, H., Henriksen, N., Higgins, A.K., 2008. From the Early Paleozoic platforms of Baltica and Laurentia to the Caledonide Orogen of Scandinavia and Greenland. Episodes 31 (1), 44–51.
Gernigon, L., Brönner, M., 2012. Late Palaeozoic architecture and evolution of the south-western Barents Sea: insights from a new generation of aeromagnetic data. J. Geol. Soc. Lond. 169 (4):449–459. http://dx.doi.org/10.1144/0016-76492011-131.
Gernigon, L., Brönner, M., Roberts, D., Olesen, O., Nasuti, A., Yamasaki, T., 2014. Crustal and basin evolution of the southwestern Barents Sea: from Caledonain orogeny to continental breakup. Tectonics 33:347–373. http://dx.doi.org/10.1002/2013TC003439.
Grad, M., Mjelde, R., Czuba, W., Guterch, A., Schweitzer, J., IPY Project Group, 2011. Modelling of seafloor multiples observed in OBS data from the North Atlantic—new seismic tool for oceanography? Pol. Polar Res. 32:405–422. http://dx.doi.org/10.2478/v10183-011-0027-3.
Grimstad, S., 2016. Salt Tectonics in the Central and Northeastern Nordkapp Basin, Barents Sea. Master Thesis. Dept. of Geol., Univ. of Oslo, Oslo, Norway.
Grogan, P., Østvedt-Ghazi, A.M., Larssen, G.B., Fotland, B., Nyberg, K., Dahlgren, S., Eidvin, T., 1999. Structural elements and petroleum geology of the Norwegian sector of the northern Barents Sea. In: Fleet, A.J., Boldy, S.A.R. (Eds.), Petroleum Geology of the Northwest Europe: Proceedings of the 5th Conference. Geological Society, London: pp. 247–259 http://dx.doi.org/10.1144/0050247.
Grogan, P., Nyberg, K., Fotland, B., Myklebust, R., Dahlgren, S., Riis, F., 2000. Cretaceous magmatism south and east of Svalbard: evidence from seismic reflection and magnetic data. Polarforschung 68, 25–34.
Gudlaugsson, S.T., Faleide, J.I., 1994. The continental margin between Spitsbergen and Bjørnøya. In: Eiken, O. (Ed.), Seismic Atlas of Western Svalbard. Medd.-Nor. Polarinst. 130, pp. 11–13.
Gudlaugsson, S.T., Faleide, J.I., Fanavoll, S., Johansen, B., 1987. Deep seismic reflection profiles across the western Barents Sea. Geophys. J. R. Astron. Soc. 89:273–278. http://dx.doi.org/10.1111/j.1365-246X.1987.tb04419.x.
Gudlaugsson, S.T., Faleide, J.I., Johansen, S.E., Breivik, A.J., 1998. Late Palaeozoic structural development of the South-western Barents Sea. Mar. Pet. Geol. 15:73–102. http://dx.doi.org/10.1016/S0264-8172(97)00048-2.
Harland, W.B., Gayer, R.A., 1972. The Arctic Caledonides and earlier oceans. Geol. Mag. 109:289–314. http://dx.doi.org/10.1017/S0016756800037717.
Harland, W.B., Anderson, L.M., Manasrah, D., 1997. The geology of Svalbard. Geol. Soc. Lond. Mem. 17, 521.
Henriksen, E., Ryseth, A.E., Larssen, G.B., Heide, T., Rønning, K., Sollid, K., Stoupakova, A.V., 2011a. Tectonostratigraphy of the greater Barents Sea: implications for petroleum systems. In: Spencer, A.M., Embry, A.F., Gautier, D.L., Stoupakova, A.V., Sørensen, K. (Eds.), Arctic Petroleum Geology. Memoirs Geological Society of London 35: pp. 163–195. http://dx.doi.org/10.1144/M35.10.
Henriksen, E., Bjørneseth, H.M., Hals, T.K., Heide, T., Kiryukhina, T., Kløvjan, O.S., Larssen, G.B., Ryseth, A.E., Rønning, K., Sollid, K., Stoupakova, A., 2011b. Uplift and erosion of the greater Barents Sea: impact on prospectivity and petroleum systems. In: Spencer, A.M., Embry, A.F., Gautier, D.L., Stoupakova, A.V., Sørensen, K. (Eds.), Arctic Petroleum Geology. Memoirs Geological Society of London 35:pp. 271–281. http://dx.doi.org/10.1144/M35.17.
Higgins, A.K., Leslie, A.G., 2000. Restoring thrusting in the East Greenland Caledonides. Geology 28:1019–1022. http://dx.doi.org/10.1130/0091-7613(2000)28<1019:RTITEG>2.0.CO;2.
Jakobsson, M., Mayer, L., Coakley, B., Dowdeswell, J.A., Forbes, S., Fridman, B., Hodnesdal, H., Noormets, R., Pedersen, R., Rebesco, M., Schenke, H.W., Zarayskaya, Y., Accettella, D., Armstrong, A., Anderson, R.M., Bienhoff, P., Camerlenghi, A., Church, I., Edwards, M., Gardner, J.V., Hall, J.K., Hell, B., Hestvik, O., Kristoffersen, Y., Marcussen, C., Mohammad, R., Mosher, D., Nghiem, S.V., Pedrosa, M.T., Travaglini, P.G., Weatherall, P., 2012. The International Bathymetric Chart of the Arctic Ocean (IBCAO) version 3.0. Geophys. Res. Lett. 39. http://dx.doi.org/10.1029/2012GL052219.
Kenyon, S., Forsberg, R., Coakley, B., 2008. New gravity field for the Arctic. Eos. Trans. AGU 89:1–2. http://dx.doi.org/10.1029/2008EO320002.
Klitzke, P., Sippel, J., Faleide, J.I., Scheck-Wenderoth, M., 2016. A 3D gravity and thermal model for the Barents Sea and Kara Sea. Tectonophysics 684:131–147. http://dx.doi.org/10.1016/j.tecto.2016.04.033.
Krysinski, L., Grad, M., Mjelde, R., Czuba, W., Guterch, A., 2013. Seismic and density structure of the lithosphere-asthenosphere system along transect Knipovich Ridge-Spitsbergen-Barents Sea—geological and petrophysical implications. Pol. Polar Res. 34 (2):111–138. http://dx.doi.org/10.2478/popore-2013-0011.
Leever, K.A., Gabrielsen, R.H., Faleide, J.I., Braathen, A., 2011. A transpressional origin for the West Spitsbergen ford-and-thrust belt: insight from analog modeling. Tectonics 30, TC2014. http://dx.doi.org/10.1029/2010TC002753.
Levshin, A.L., Schweitzer, J., Weidle, C., Shapiro, N.M., Ritzwoller, M.H., 2007. Surface wave tomography of the Barents Sea and surrounding regions. Geophys. J. Int. 170: 441–459. http://dx.doi.org/10.1111/j.1365-246X.2006.03285.x.
Lorenz, H., Gee, D.G., Whitehouse, M.J., 2007. New geochronological data on Palaeozoic igneous activity and deformation in the Severnaya Zemlya Archipelago, Russia, and implications for the development of the Eurasian Arctic margin. Geol. Mag. 144: 105–125. http://dx.doi.org/10.1017/S001675680600272X.
Ludwig, W.I., Nafe, J.E., Drake, C.L., 1970. Seismic refraction. Sea 4 (1), 53–84.
Marello, L., Ebbing, J., Gernigon, L., 2010. Magnetic basement study in the Barents Sea from inversion and forward modelling. Tectonophysics 493:153–171. http://dx.doi.org/10.1016/j.tecto.2010.07.014.
Marello, L., Ebbing, J., Gernigon, L., 2013. Basement inhomegenities and crustal setting in the Barents Sea from a combined 3D gravity and magnetic model. Geophys. J. Int. 193:557–584. http://dx.doi.org/10.1093/gji/ggt018.
Minakov, A., Mjelde, R., Faleide, J.I., Flueh, E.R., Dannowski, A., Keers, H., 2012. Mafic intrusions east of Svalbard imaged by active-source seismic tomography. Tectonophysics 518–521:106–118. http://dx.doi.org/10.1016/j.tecto.2011.11.015.
Minakov, A., Bretel, P., Lebedeva-Ivanova, N., Meyer, O., 2014. Cruise Report: Barents OBS 2014, Ocean Bottom Survey in the Barents Sea, University of Oslo Report (35 pp.).
Ohm, S.E., Karlsen, D.A., Austin, T.J.F., 2008. Geochemically driven exploration models in uplifted areas: examples from the Norwegian Barents Sea. AAPG Bull. 92 (9): 1191–1223. http://dx.doi.org/10.1306/06180808028.
Olovyanishnikov, V.G., Siedlecka, A., Roberts, D., 1997. Aspects of geology of the Timans, Russia and linkage with Varanger Peninsula, NE Norway. Bulletin of the Geological Survey of Norway 433, pp. 28–29.
Polteau, S., Hendriks, B.W.H., Planke, S., Ganerød, M., Corfu, F., Faleide, J.I., Midtkandal, I., Svensen, H.S., Myklebust, R., 2016. The Early Cretaceous Barents Sea Sill Complex: distribution, $^{40}Ar/^{39}Ar$ geochronology, and implications for carbon gas formation. Palaeogeogr. Palaeoclimatol. Palaeoecol. 441:83–95. http://dx.doi.org/10.1016/j.palaeo.2015.07.007.
Ritzmann, O., Faleide, J.I., 2007. Caledonian basement of the western Barents Sea. Tectonics 26 (5):1–20. http://dx.doi.org/10.1029/2006TC002059 TC5014.
Roberts, D., Gee, D.G., 1985. An introduction to the structure of the Scandinavian Caledonides. In: Gee, D.G., Sturt, B.A. (Eds.), The Caledonide Orogen—Scandinavia and Related Areas. John Wiley & Sons, Chichester, pp. 55–68.
Roberts, D., Olovyanishnikov, V., 2004. Structural and tectonic development of the Timanide orogen. In: Gee, D.G., Pease, V. (Eds.), The Neoproterozoic Timanide Orogen of Eastern Baltica. Memoirs Geological Society of London 30:pp. 47–57. http://dx.doi.org/10.1144/GSL.MEM.2004.030.01.05.
Roberts, D., Siedlecka, A., 2002. Timanian orogenic deformation along the northeastern margin of Baltica, Northwest Russia and Northeast Norway, and Avalonia-Cadomian connections. Tectonophysics 352 (1–2):169–184. http://dx.doi.org/10.1016/S0040-1951(02)00195-6.
Smelror, M., Petrov, O., Larsen, G.B., Werner, S.C., 2009. Atlas: Geological History of the Barents Sea. Geological Survey of Norway, Trondheim.
Torsvik, T.H., Van der Voo, R., Meert, J.G., Mosar, J., Walderhaug, H.J., 2001. Reconstructions of the continents around the North Atlantic at about the 60th parallel. Earth Planet. Sci. Lett. 187:55–69. http://dx.doi.org/10.1016/S0012-821X(01)00284-9.
Wessel, P., Smith, W.H.F., 1998. New, improved version of generic mapping tools released. EOS Trans. Am. Geophys. Union 79:579. http://dx.doi.org/10.1029/98EO00426.
Zelt, C.A., Forsyth, D.A., 1994. Modeling wide-angle seismic data for crustal structure: southeastern Grenville Province. J. Geophys. Res. 99 (B6):11687–11704. http://dx.doi.org/10.1029/93JB02764.
Zelt, C.A., Smith, R.B., 1992. Seismic traveltime inversion from 2-D crustal velocity structure. Geophys. J. Int. 108:16–34. http://dx.doi.org/10.1111/j.1365-246X.1992.tb00836.x.
Ziegler, P.A., 1988. Evolution of the Arctic-North Atlantic and the Western Tethys. AAPG Memoirs, Tulsa 43 pp. 1–198.

3. Synthesis

This thesis focuses on the crustal structure of the western Barents Sea and how structural inheritance from the Caledonian orogeny has influenced the subsequent basin formation. Our research provides an increased understanding of the large-scale processes responsible for the evolution of the region. In the following sections we synthesize and discuss the main findings of the present study, and assess their implications for understanding Caledonian trends in the western Barents Sea.

3.1 Synthesis of main findings and key implications

Our main findings along the modeled profiles are indicated in Fig. 5 and are summarized in eight points: **(1)** The Laurentia-Baltica suture interpreted on profile 1 coincides with an area of highly stretched and thinned continental crust and follows the major fault systems west of Loppa High, consistent with the findings of Clark et al. (2013). **(2)** The observed magnetic anomalies along profile 1 correlates with an area of high velocities and densities modeled in the lower crust beneath and east of Loppa High. These observations support the location of the Caledonian deformation front as interpreted from magnetic anomalies (Gernigon and Brönner, 2012; Gernigon et al., 2014, Fig. 6). **(3)** The proposed location of the N-S trending Caledonian suture on profile 2 is based on lateral variations in the crystalline crust where a westward dipping suture separates lower velocities in Laurentia (6.0-6.4 km/s) from higher velocities in Barentsia (6.2-6.7 km/s). This is consistent with velocities modeled by Breivik et al. (2003) along OBS profile 3e (Fig. 7). **(4)** A rapid drop in Moho depth (from 27 km to 33 km depth) in central parts of profile 1 creates a crustal root. A similar root structure has been modeled beneath the Olga Basin region (Breivik et al., 2002; Fig. 7 and interpreted as a proto-Caledonian subduction zone dipping to the southeast with the crustal root representing a remnant of continental collision between Baltica and Barentsia. In this scenario Barentsia acts as an independent microcontinent between Laurentia and Baltica. **(5)** A change in reflective character is

observed across the proposed Baltica-Barentsia suture, both from the modeled OBS data and from vintage MCS data. This indicates crustal units with different physical properties, expressed as a change from a reflective crystalline crust within Barentsia to a more transparent crust in Baltica. The idea of Barentsia as a microcontinent has also been supported by magnetic modeling (Marello et al., 2013) as the block is characterized by low magnetic properties compared to its surroundings. **(6)** Early Cretaceous magmatism related to the High Arctic Large Igneous province have been mapped both south (Polteau et al., 2016) and east of Svalbard (Minakov et al., 2012; 2017) and the sill intrusion modeled along profile 2 could be related to this event. **(7)** The lower crustal body (LCB) interpreted in the western part of profile 3 is proposed to be related to the western LCB modeled by Krysiński et al. (2013) beneath Sørkapp. The double magnetic anomaly observed in the westernmost part of the model is most likely related to a Proterozoic granitic gneiss terrain onshore Svalbard. **(8)** The seismic activity in Storfjorden is interpreted to occur along NE-SW oriented strike slip faults (e.g. Pirli et al., 2013; Ottemöller et al., 2014) and is located in the proximity of the magnetic anomalies. We propose that these NE-SW oriented faults represent an old zone of weakness in the crystalline crust with compositional and rheological variations, that combined with thermal and post-glacial uplift could explain the recent seismic activity.

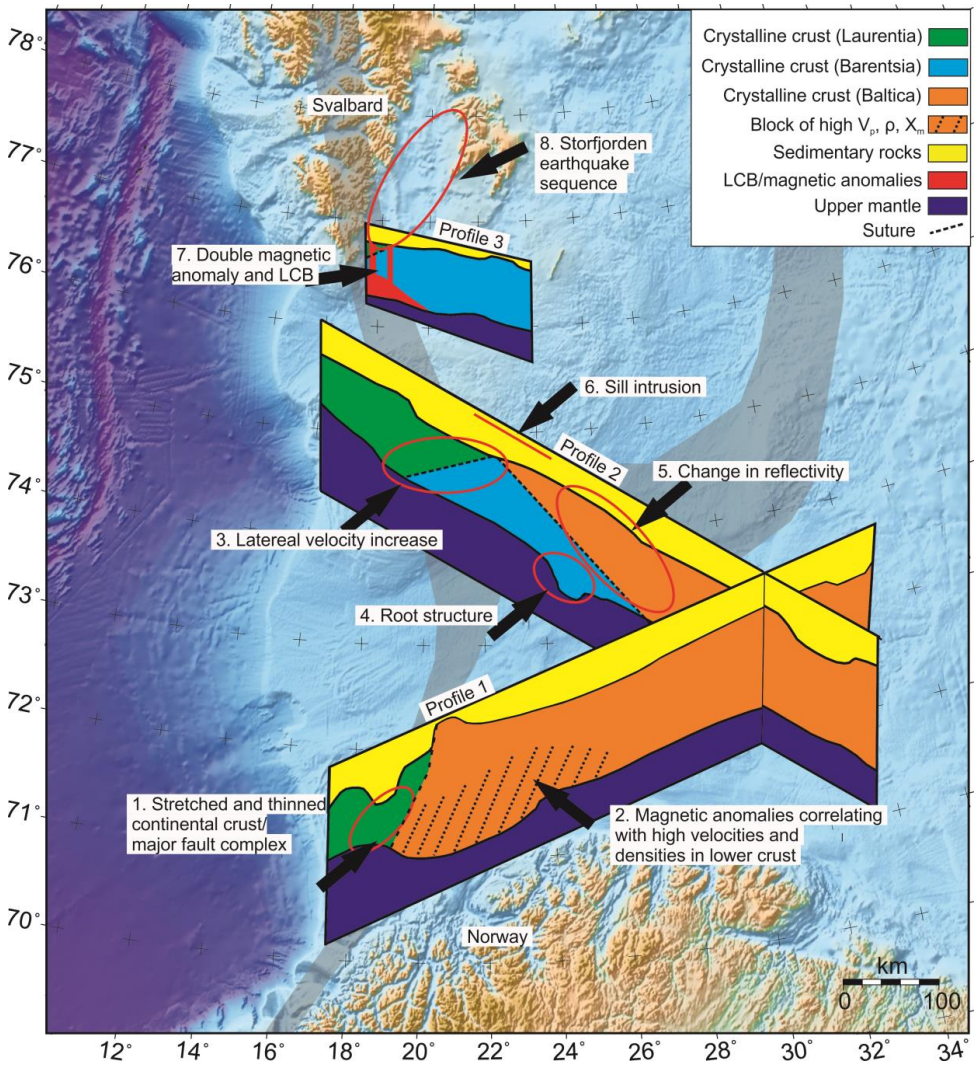

***Figure 5**: Schematic illustration of the main findings along the modeled profiles. Gray areas indicate the location of the proposed Caledonian suture zones.*

3.1.1 Caledonian suture and deformation front

The westernmost part of the Barents Sea is underlain by Caledonian basement rocks, but the eastern limit of the Caledonian suture and deformation front is not well constrained (e.g. Gudlaugsson et al., 1998; Breivik et al., 2005; Gee et al., 2006; Barrère et al., 2009: Henriksen et al., 2011a; Gasser, 2014).

Caledonian rocks have been found on Kvitøya (easternmost Svalbard, Fig. 2) but are absent on Franz Josef Land (Dibner, 1998; Pease et al., 2001). NW-SE striking Timanian basement is exposed on the Varanger Peninsula in northern Norway and offshore geophysical studies indicate that Timanian basement rock extends from the eastern and into the central Barents Sea (Ritzmann and Faleide, 2009; Marello et al., 2010, 2013; Gernigon and Brönner, 2012). Evidence favoring Timanian basement has been identified in a deep drill-hole on Alexandra Island in westernmost Franz Josef Land (Dibner, 1998; Pease et al., 2001). These findings led Gee et al. (2006) to the conclusion that a Caledonian suture must lie between Kvitøya and Franz Josef Land and that the Caledonian deformation front lies east of Franz Josef Land.

An N-S oriented suture through Svalbard is suggested from deep seismic and potential field data (Gudlaugsson et al., 1987, 1998; Breivik et al., 2003; 2005, Ritzmann and Faleide, 2007; Krysiński et al., 2013). *The location of this suture is supported by the lateral velocity variations modeled along profile 2 (Figs. 5, 6), indicating a transition from low to high velocities across the suture* (research question 1).

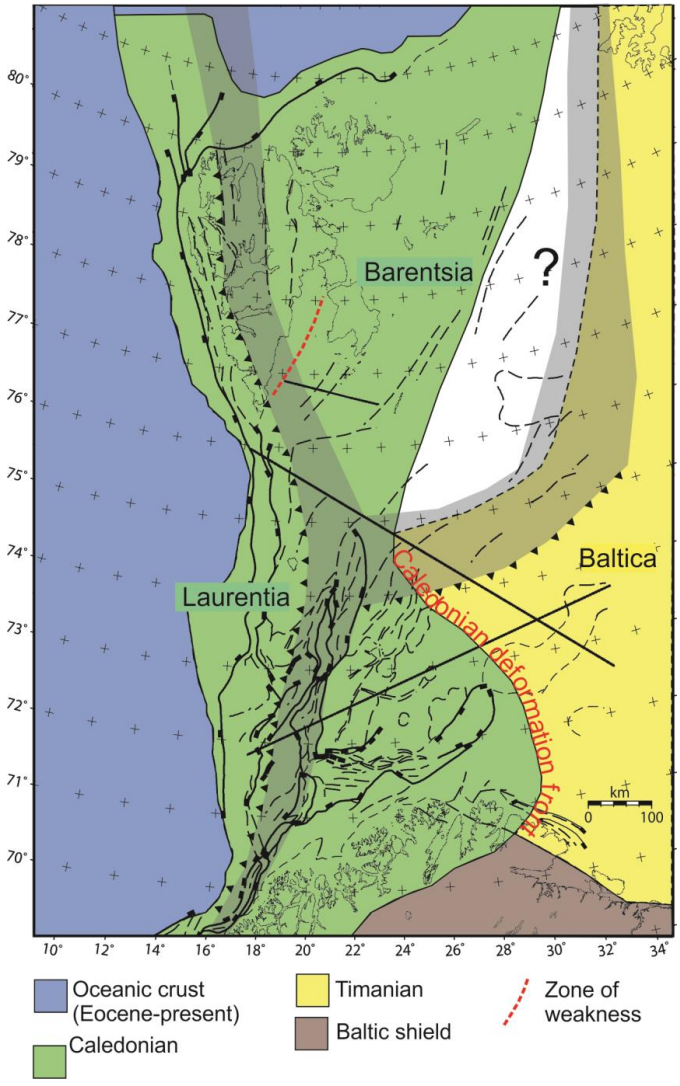

***Figure 6**: Basement domains of the western Barents Sea with proposed location of Caledonian sutures (shaded area) and deformation front. White areas are unresolved. Modified from Faleide et al. (2017).*

Additionally, a NE-SW trending Caledonian branch between Svalbard and Franz Josef Land has been suggested (Gudlaugsson et al., 1998; Breivik et al., 2002, Marello et al., 2010, 2013). In this scenario, Barentsia (parts of Svalbard and adjacent parts of the Barents Sea) acts as a microcontinent between Laurentia and Baltica. *The change in reflective character and the crustal root modeled along profile 2 supports the location of the Baltica-Barentsia suture as suggested by previous studies and adds further constraints of where this branch meets the N-S oriented suture* (research question 2, Fig. 6*)*. The southern boundary of the Barentsia microcontinent is not well constrained from previous studies, and the main objective for acquiring profile 1 was to provide these constraints. However, no evidence of a Baltica-Barentsia suture could be identified from along profile 1 *and if the suture exists it is located north of profile 1* (research question 2). The main findings from the modeling along profile 1 (paper 2) is that the high velocities and densities in the lower crust beneath and east of Loppa High correlates with the positive magnetic anomalies in the area. This indicates that the upper basement structures may not have significantly affected the magnetic anomaly pattern. The western part of profile 1 is characterized by higher velocities and densities as well as a positive magnetic anomaly, compared to the eastern part, indicating two different basement domains. *The transition between these two domains correlates well with the position of the Caledonian deformation front proposed from magnetic data* (Gernigon and Brönner, 2012; Fig. 6, research question 1).

3.1.2 Early post-Caledonian basin formation

Early post-Caledonian graben formation resulted in N-S oriented Devonian basins on Spitsbergen, Svalbard (e.g. Manby and Lyberis, 1992), but Devonian basins in the Barents Sea are poorly resolved. Any Devonian (meta) sedimentary rocks in the Barents Sea are expected to have velocities and densities approaching those of crystalline rocks, and are therefore difficult to map by use of seismic data. Based on

magnetic data, it has been suggested that the first phase of post-Caledonian orogenic collapse and subsequent rifting had a predominantly NNW-SSE trend compared to the later NE-SW trend seen in the Carboniferous rift phase, and that this was determined by the original Caledonian structural grain (Gernigon and Brönner, 2012; Gernigon et al. 2014). The "Scott Hansen Complex" is proposed to be a NNW-SSE oriented Devonian basin in the southwestern Barents Sea (Gernigon and Brönner, 2012). However, the rifting initiated in the Carboniferous is the oldest that has been constrained by reflection seismic data, creating NE-striking, evaporite-filled basins, such as Nordkapp and Ottar Basins (Breivik et al., 1995; Gudlaugsson et al., 1998).

Profile 1 and profile 2 crosses the Ottar and Sørkapp basins, respectively, but their outline is not well constrained by the OBS data. However, a spatially distinct negative gravity anomaly is observed across the Ottar Basin, probably due to the presence of salt (Breivik et al., 1995). Nearby seismic profiles are needed to discuss the orientation of the basins, and comparing our model with the findings of Clark et al. (2013) and Breivik et al. (2003) *we support a NE-SW orientation of the Carboniferous rift basins, as proposed by earlier studies* (Breivik et al., 1995; Gudlaugsson et al. 1998; Breivik et al., 2005, research question 3). Additionally, the Nordkapp Basin can be observed from gravity data as having a clear NE-SW orientation.

A Devonian basin trend oriented NNW-SSE as proposed by Gernigon and Brönner (2012) is unresolved by our data and the pattern of the earliest post-Caledonian collapse and extension remains elusive (research question 3). The NE-SW Carboniferous rift structures in the southwestern Barents Sea (Nordkapp and Ottar basins) are oriented almost perpendicular to the NNW-SSE trend of the magnetic anomalies.

3.1.3 The Storfjorden earthquake sequence

The Storfjorden earthquake sequence was initiated by an $M_w = 6.1$ event on 21 February 2008 and lasted until 2016. The distribution of earthquakes and faults plane solutions (Pirli et al., 2013; Ottemöller et al., 2014) indicate that the main $M_w = 6.1$ event and the majority of the subsequent earthquakes are related to rupture along NE-SW oriented strike-slip faults in Storfjorden. However, the major faults systems mapped onshore Svalbard, such as the Billefjorden Fault Zone and the Lomfjorden Faults Zone, have a predominantly N-S orientation (e.g. Harland et al., 1974; Bælum and Braathen, 2012). These fault systems are believed to continue southwards, but their extension into Storfjorden is not well resolved (e.g. Skilbrei, 1992; Breivik et al., 2005).

NE-SW oriented faults in Storfjorden that could be associated with the seismic activity have not been properly mapped. OBS profile 3 crosses the main cluster of the earthquake sequence. The continuation of a Cenozoic shear south of Sørkapp proposed by Bergh and Grogan (2003) fits well with the earthquake locations and fault plate solutions, but the northeastward extension of this zone lies beyond the area of ray coverage in the OBS data and remains uncertain.

A double magnetic anomaly observed in the westernmost part of profile 3 has been modeled as two magnetic blocks within the crystalline crust. Our model indicates a heterogeneous crust in the western part, which is located close to the earthquake sequence. *We suggest that the crust here has compositional and rheological variations that represent an old NE-SW oriented zone of weakness, possibly of Caledonian age. This zone of weakness, combined with the N-S oriented Caledonian suture and thermal and post-glacial uplift, may explain the recent seismic activity in Storfjorden* (research question 4).

3.2 Concluding remarks

The aim of this study has been to increase the understanding of Caledonian structures in the southwestern Barents Sea, and how these have affected the subsequent tectonic evolution in the area. This has been achieved by travel-time modeling of two regional (~650 km) ocean bottom seismometer profiles across the southwestern Barents Sea, in addition to a shorter (~170 km) profile across Storfjorden. The seismic models are combined with gravity and magnetic models.

- Our models supports the existence of a separate NE-SW Caledonian trend into the central Barents Sea, branching off the N-S trending Svalbard Caledonides, implying the existence of Barentsia as an independent microcontinent between Laurentia and Baltica.
- Lateral velocity and density variations in the crystalline crust beneath and east of Loppa High are interpreted as a transition from Caledonian basement in the west to Timanian basement in the east.
- Magnetic anomalies correlate well with high velocities and densities in the lower crust beneath Loppa High, suggesting that upper-crustal basement structures may not have significantly affected the magnetic anomaly pattern, and may therefore not necessarily constrain the early post-Caledonian basin formation.
- Our models support a NE-SW orientation of Carboniferous rift basins.
- The earliest post-Caledonian (Devonian) collapse and subsequent extension remains poorly resolved in the seismic data and requires better documentation.
- Compositional and rheological variations in the crystalline crust beneath Storfjorden are interpreted to represent an old zone of weakness, possibly of Caledonian age. This zone of weakness, combined with the N-S oriented Caledonian suture and the present-day uplift of the region, could explain the recent seismic activity in Storfjorden.

3.3 Future perspectives

3.3.1 S-wave modeling and land station data

Only P-waves have been modeled as part of this thesis. S-wave travel-time modeling has the potential to provide additional information on lithology and mineralogical composition of the crust, in addition to seismic anisotropy, and should be done in the future to increase the understanding of the composition and structure of the crystalline crust and upper mantle. The standard modeling approach is to keep the boundaries in the existing P-wave model constant, and only vary the Vp/Vs ratios and the converting boundaries until a satisfactory match is achieved (Mjelde et al., 2002).

A relationship between V_p/V_s ratios and lithology have been established from laboratory experiments and cases studies (e.g. Neidell, 1985; Tatham, 1985; Tatham and McCormac, 1991; Christensen, 1996). Most rock forming minerals have V_p/V_s ratios from 1.7 to 1.9, while quartz has a value of 1.48 (Birch, 1961), which makes the V_p/V_s ratio particularly sensitive to the content of quartz. The V_p/V_s ratio can therefore be used to distinguish between felsic (quartz rich) and mafic (quartz poor) crystalline rocks. OBS data have proven to be useful in lithological prediction both at the Lofoten (Mjelde and Sellevoll, 1993; Mjelde et al., 1993, 1996) and Vøring Margin (Digranes et al., 1996, 1998; Mjelde et al., 2003).

S-waves are also known to be sensitive to micro-cracks aligned by the present day stress field (Crampin, 1990). In such an anisotropic medium an S-wave will split into two waves, one polarized along the cracks, and one polarized perpendicular to the cracks propagating with a slower velocity (Mjelde et al., 2003), and can thus be used to investigate the anisotropy of rocks.

In addition to S-waves, recording from two permanent seismic stations are available. The seismic stations on Hornsund and Hopen lie in the northwestward and

southeastward continuation of profile 3, respectively, and the model can be extended to include these data. The land stations recordings will most likely provide important information about the structure of the lower crust and Moho geometry along profile 3 in Storfjorden. However, the recordings from Hornsund are arranged in an array and including these data in the model involves an extensive amount of work and is beyond the scope of this thesis. Records from the land seismic stations are expected to provide wide-angle reflections from Moho and far-offset refractions from the upper mantle. These arrivals can be used in amplitude modeling to better constrain the velocity contrast across Moho and the velocity gradient in the upper mantle.

3.3.2 Seismic tomography and full waveform inversion

First-arrival travel-time tomography (e.g. Korenaga et al., 2000) is a method commonly used for wide-angle seismic data. It has not been applied in this thesis, but using several different modeling methods could increase the robustness of the models and should be considered. The main advantage of this method is that the modeler does not need to assign picked travel-times to certain layers, resulting in a more objective model. On the other hand, first-arrival models do not include all the information recorded by the ocean bottom seismometers (e.g. Minshull, 2009).Travel-time residuals between picked and calculated first arrivals combined with the partial derivatives of travel-times with respect to the model parameters are used to solve the inverse problem. This is done using a least squares method. The Rayinvr model can be used as input for tomographic inversion, and after using an iterative inversion approach the resulting seismic tomography model will be damped and smoothed.

Full waveform inversion (FWI) makes use of all information recorded in seismic data, including travel-times, amplitudes, multiples and diffractions. The FWI method often provides sharper and higher resolution images than conventional travel-time

tomography (e.g. Tarantola, 1984). It requires large computer resources and has therefore been considered to be of limited practical use. However, recent development of faster computers, more efficient inversion methods (e.g. Pratt, 1999; Jakobsen and Ursin, 2015) and an increasing demand for more detailed imaging have made FWI more popular. Full waveform inversion requires a good starting model, often obtained from travel-time modeling, and the velocity models from this study could be used as input to FWI to obtain more detailed information about the subsurface.

3.3.3 2D and 3D forward and thermal isostatic modeling

2D and 3D forward and thermal isostatic modeling of multi-stage rifting can be used to examine the role of pre-existing structural inheritance, crustal strength and thickness variation. Numerical modeling studies (e.g. Huismans and Beaumont, 2011; Allken et al., 2012, 2013) demonstrate that pre-existing weaknesses favorably oriented tend to be reactivated, whereas structures at a highly oblique angle tend to be ignored. Moderately oblique inherited structures are expected to result in oblique reactivation. However, the present quantitative understanding of the role of oblique inheritance and factors controlling oblique reactivation and subsequent extensional basin formation is limited. A 2D and 3D forward and thermal isostatic modeling study is planned for the western Barents Sea. This study will investigate the role of pre-existing structural weaknesses with varying obliquity and crustal strength on the formation of rift basins. Such an integrated approach is important in improving the understanding of large-scale processes responsible for multi-stage Palaeozoic basin formation in the western Barents Sea.

3.3.4 New OBS surveys

A more densely spaced grid of ocean bottom seismometer data is needed to further constrain the Caledonian suture and deformation front in the Barents Sea. Fig. 7 shows existing OBS profiles in the western Barents Sea and proposed locations for new OBS profiles. The northern profile can be used to constrain northeastern extension of the proposed Baltica-Barentsia suture through the central Barents Sea. The southern profile should be acquired across the Ottar Basin and/or the Scott Hansen Complex in the southwestern Barents Sea, in order to increase the understanding of how the Caledonian nappes and deformation front have influenced earliest post-Caledonian basin formation. All existing OBS profiles could be combined to produce an updated map of top basement and Moho and sum up the present knowledge. This could be used to identify remaining gaps in the understanding of the post-Caledonian evolution of the western Barents Sea. Additionally, 3D gravity and magnetic modeling based on the existing (and new) OBS profiles should be done.

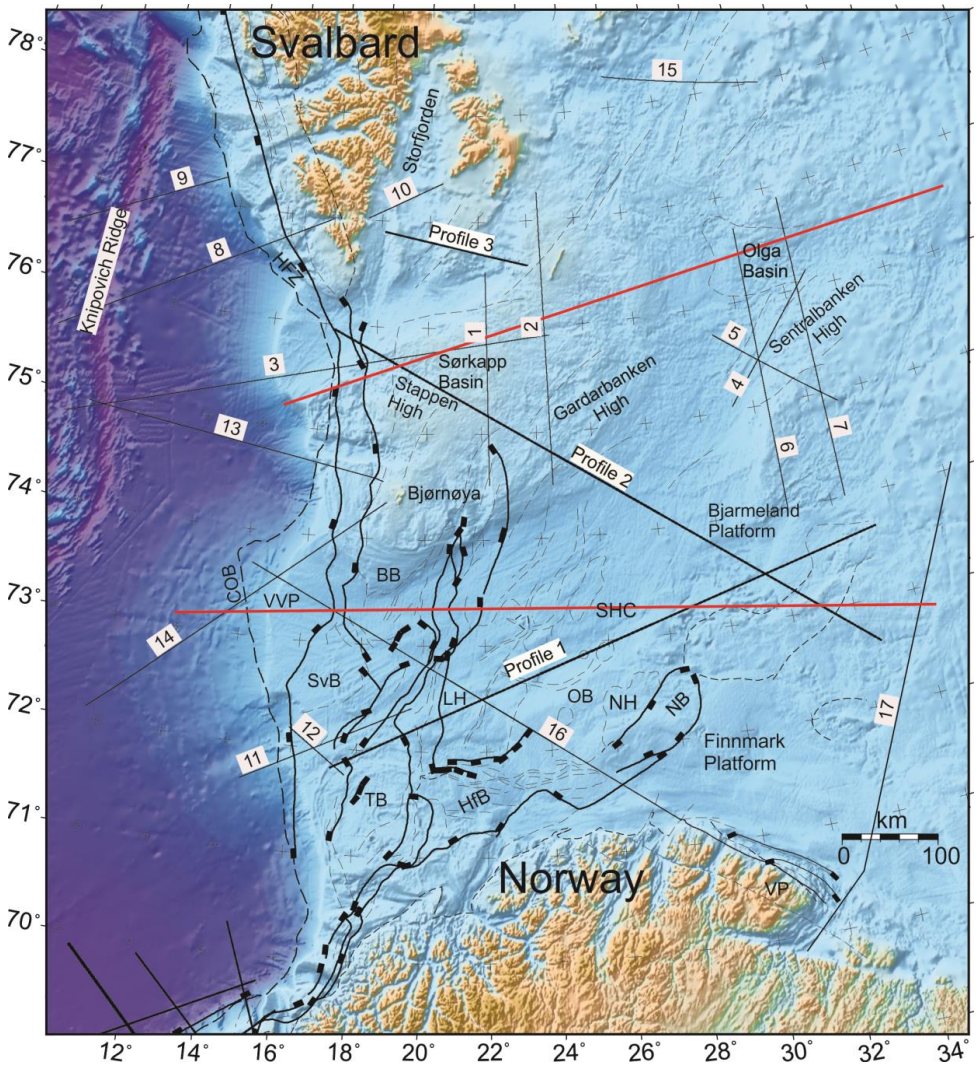

***Figure 7**: Location of existing OBS profiles (numbered 1-17), profile 1-3 from the 2014 dataset (this study) and suggested locations of new OBS profiles (in red). See Fig. 2 for abbreviations.*

4 References cited in Introduction and Synthesis

Allken, V., Huismans, R. S., Thieulot, C., 2012. Factors controlling the mode of rift interaction in brittle-ductile coupled systems: A 3D numerical study. Geochem. Geophys. Geosyst. 13, Q05010, doi:10.1029/2012GC004077.

Allken, V., Huismans, R. S., Fossen, H., Thieulot, C., 2013. 3D numerical modelling of graben interaction and linkage: a case study of the Canyonlands grabens, Utah. Basin Research 25, 1-12, 10.1111/bre.12010.

Barrère, C., Ebbing, J., Gernigon, L., 2009. Offshore prolongation of Caledonian structures and basement characterization in the western Barents Sea from geophysical modelling. Tectonophysics 470, 71-88.

Bergh, S. G., Grogan, P., 2003. Tertiary structure of the Sørkapp-Hornsund region, south Spitsbergen, and implications for the offshore southern extension of the fold-thrust Belt. Norwegian Journal of Geology 83, 43-60.

Birch, F., 1961. The velocity of compressional waves in rocks to 10 kilobars: Part 2. J. Geophys. Res. 66, 2199-2224.

Breivik, A. J, Gudlaugsson, S. T., Faleide, J. I., 1995. Ottar Basin, SW Barents Sea: a major Upper Plaeozoic rift basin containing large volumes of deeply buried salt. Basin Research 7, 299-312.

Breivik, A. J., Faleide, J. I., Gudlaugsson, S. T., 1998. Southwestern Barents Sea margin: late Mesozoic sedimentary basins and crustal extension. Tectonophysics 293, 21-44, http://dx.doi.org/10.1016/S0040-1951(98)00073-0.

Breivik, A. J., Verhoef, J., Faleide, J. I., 1999. Effect of thermal contrasts on gravity modeling at passive margins: results from the western Barents Sea. J. Geophys. Res. 104 (B7), 15293-15311, 10.1029/1998JB900022.

Breivik, A. J., Mjelde, R., Grogan, P., Shimamura, H., Murai, Y., Nishimura, Y., Kuwano, A., 2002. A possible Caledonide arm through the Barents Sea imaged by OBS data. Tectonophysics 355, 67-97, http://dx.doi.org/10.1016/S0040-1951(02)00135-X.

Breivik, A. J., Mjelde, R., Grogan, P., Shimamura, H., Murai, Y., Nishimura, Y., 2003. Crustal structure and transform margin development south of Svalbard based on ocean bottom seismometer data. Tectonophysics 369, 37-70, http://dx.doi.org/10.1016/S0040-1951(03)00131-8.

Breivik, A. J., Mjelde, R., Grogan, P., Shimamura, H., Murai, Y., Nishimura, Y., 2005. Caledonide development offshore-onshore Svalbard based on ocean bottom seismometer, conventional seismic, and potential field data. Tectonophysics 401, 79-117, http://dx.doi.org/10.1016/j.tecto.2005.03.009.

Bælum, K., Braathen, A., 2012. Along-strike changes in fault array and rift basin geometry of the Carboniferous Billefjorden Trough, Svalbard, Norway. Tectonophysics 546-547, 38-55.

Clark, S. A., Faleide, J. I., Hauser, J., Ritzmann, O., Mjelde, R., Ebbing, J., Thybo, H., Flüh, E., 2013. Stochastic velocity inversion of seismic reflection/refraction traveltime data for rift structure of the southwest Barents Sea. Tectonophysics 593, 135-150, https://doi.org/10.1016/j.tecto.2013.02.033.

Christensen, N.I., 1996. Poisson's ratio and crustal seismology. J. Geophys. Res. 101 (B2), 3139-3156.

Crampin, S., 1990. The scattering of S-waves in the crust. PAGEOPH 132, 67-91.

Dibner, V.D., 1998. The geology of Franz Joseph Land – an introduction. In: Solheim, A., Musatov, E., Heintz, N. (Eds.) Geological Aspects of Franz Joseph Land and the Northernmost Barents Sea. Norsk Polarinstitutt Meddelelser 151, 24-46.

Digranes, P., Mjelde, R., Kodira, S., Shimamura, H., Kanazawa, T., Shiobara, H., Berg, E.W., 1996. Modelling Shear Waves in OBS data from the Vøring Basin (Northern Norway) by 2-D Ray-tracing. Pure and applied geophysics 147 (4), 611-629.

Digranes, P., Mjelde, R., Kodira, S., Shimamura, H., Kanazawa, T., Shiobara, H., Berg, E.W., 1998. A regional share-wave velocity model in the central Vøring Basin, N. Norway, using three-component Ocean Bottom Seismographs. Tectonophysics 293, 157-174.

Dimakis, P., Braathen, B.I., Faleide, J.I., Elverhøi, A., Gudlaugsson, S.T., 1998. Cenozoic erosion and the preglacial uplift of the Svalbard-Barents Sea region. Tectonophysics 300, 311-327, http://dx.doi.org/10.1016/S0040-1951(98)00245-5.

Doré, A.G., 1991. The structural foundation and evolution of Mesozoic seaways between Europe and the Arctic. Palaeogeogr. Palaeoclimatol. Palaeoecol. 87, 441-492, https://doi.org/10.1016/0031-0182(91)90144-G.

Drachev, S., Saunders, A., 2006. The Early Cretaceous Arctic LIP: its geodynamic setting and implications for Canada Basin opening. In: Proceedings of the Forth International Conference on Arctic Margins, US Department of the Interior, Anchorage, 216-223.

Faleide, J. I., Vågnes, E, Gudlaugsson, S. T., 1993. Late Mesozoic-Cenozoic evolution of the south-western Barents Sea in a regional rift-shear tectonic setting. Mar. Pet. Geol. 10, 186-214, https://doi.org/10.1016/0264-8172(93)90104-Z.

Faleide, J.I., Tsikalas, F., Breivik, A.J., Mjelde, R., Ritzmann, O., Engen, O., Wilson, J., Eldholm, O., 2008. Structure and evolution of the continental margin off Norway and Barents Sea. Episodes 31 (1), 82-91.

Faleide, J. I., Bjørlykke, K., Gabrielsen, R. H., 2010. Geology of the Norwegian continental Shelf. In: Bjørlykke, K. (ed.), Petroleum Geoscience: from Sedimentary Environments to Rock Physics. Springer-Verlag, Berlin Heidelberg, pp 467-499.

Faleide, J. I., Pease, V., Curtis, M. Klitzke, P., Minakov, A., Scheck-Wenderoth, M., Kostyuchenko, S., Zayonchek, A., 2017. Tectonic implications of the lithospheric structure across the Barents and Kara shelves. In: Pease, V., Coakley, B. (eds.) Circum-Arctic Lithosphere Evolution. Geological Society, London, Special Publications, 460, https://doi.org/10.1144/SP460.18

Gasser, D., 2014. The Caledonides of Greenland, Svalbard and other Arctic areas: status of research and open questions. In: Corfu, F., Gasser, D., Chew, D. M. (eds.). New Perspectives on the Caledonides of Scandinavia and Related Areas. Geological Society, London, Special Publications 390, 93-129, https://doi.org/10.1144/SP390.17.

Gabrielsen, R.H., 1984. Long-lived fault zones and their influence on the tectonic development of the southwestern Barents Sea. Journal of the Geological Society, London 141, 651-662, 10.1144/gsjgs.141.4.0651.

Gabrielsen, R. H., Færseth, R. B., Jensen, L., Kalheim, J. E., Riis, F., 1990. Structural elements of the Norwegian continental shelf: Part 1. The Barents Sea Region. NDP Bull., vol. 6. Nor. Petrol. Dir., Stavanger, Norway.

Gee, D. G., Bogolepova, O. K., Lorenz, H., 2006. The Timanide, Caledonide and Uralide orogens in the Eurasian high Arctic, and relationships to the palaeo-continents Laurentia, Baltica and Siberia. In: Gee, D.G., and Stephenson, R.A. (eds.) European Lithosphere Dynamics. Memoirs Geological Society of London 32, 507-520.

Geosoft, Oasis Montaj Software 70, Geosoft Inc., Copyright 2008.

Gernigon, L., Brönner, M., 2012. Late Palaeozoic architecture and evolution of the southwestern Barents Sea: insights from a new generation of aeromagnetic data, J. Geol. Soc. London, 169 (4), 449-459, 10.1144/0016-76492011-131.

Gernigon, L., Brönner, M., Roberts, D., Olesen, O., Nasuti, A., Yamasaki, T., 2014. Crustal and basin evolution of the southwestern Barents Sea: From Caledonian orogeny to continental breakup. Tectonics 33, 347-373, 10.1002/2013TC003439.

Gudlaugsson, S.T., Faleide, J.I., Fanavoll, S., Johansen, B., 1987. Deep seismic reflection profiles across the western Barents Sea. Geophys. J. R. Astron. Soc., 89, 273-278, https://doi.org/10.1111/j.1365-246X.1987.tb04419.x.

Gudlaugsson, S. T., Faleide, J. I., Johansen, S. E, Breivik, A. J., 1998. Late Palaeozoic structural development of the South-western Barents Sea. Marine and Petroleum Geology 15, 73-102, https://doi.org/10.1016/S0264-8172(97)00048-2.

Harland, W. B., Gayer, R.A., 1972. The Arctic Caledonides and earlier oceans. Geological Magazine 109, 289-314, https://doi.org/10.1017/S0016756800037717.

Harland, W. B., Cutbill, J. L., Friend, P., Gobbett, D. J., Holliday, D. W., Maton, P. I., Parker, J. R., Wallis, R. H., 1974. The Billefjorden Fault Zone, Spitsbergen – the long history of a major tectonic lineament. Norsk Polarinstitutt Skrifter 161, 1-72.

Henriksen, E., Ryseth, A. E., Larssen, G. B., Heide, T., Rønning, K., Sollid, K., Stoupakova, A. V., 2011a. Tectonostratigraphy of the greater Barents Sea: implications for petroleum systems. In: Spencer, A. M., Embry, A. F., Gautier, D. L., Stoupakova, A. V., Sørensen, K. (eds.) Arctic Petroleum Geology. Memoirs Geological Society of London 35, 163-195, 10.1144/M35.10.

Henriksen, E., Bjørneseth, H. M., Hals, T. K., Heide, T., Kiryukhina, T., Kløvjan, O. S., Larssen, G. B., Ryseth, A. E., Rønning, K., Sollid, K., Stoupakova, A., 2011b. Uplift and erosion of the greater Barents Sea: impact on prospectivity and petroleum systems. In: Spencer, A. M., Embry, A. F., Gautier, D. L., Stoupakova, A. V., Sørensen, K. (eds.) Arctic Petroleum Geology. Memoirs Geological Society of London 35, 271-281, 10.1144/M35.17

Huismans, R., Beaumont, C., 2011. Depth-dependent extension, two-stage breakup and cratonic underplating at rifted margins. Nature 473, 74-78, 10.1038/nature09988.

Jakobsen, M., Ursin, B., 2015. Full waveform inversion in the frequency domain using direct iterative T-matrix methods. J. Geophys. Eng. 12, 400-418, 10.1088/1742-2132/12/3/400.

Jakobsson, M., Mayer L., Coakley B., Dowdeswell, J. A., Forbes, S., Fridman, B., Hodnesdal, H., Noormets, R., Pedersen, R., Rebesco, M., Schenke, H. W., Zarayskaya, Y., Accettella, D., Armstrong, A., Anderson, R. M., Bienhoff, P., Camerlenghi, A., Church, I., Edwards, M., Gardner J. V., Hall, J. K., Hell, B., Hestvik, O., Kristoffersen, Y., Marcussen, C., Mohammad, R., Mosher, D., Nghiem, S. V., Pedrosa, M. T., Travaglini, P. G., Weatherall, P., 2012. The International Bathymetric Chart of the Arctic Ocean (IBCAO) Version 3.0. Geophys. Res. Lett. 39, 10.1029/2012GL052219.

Klitzke, P., Sippel, J., Faleide, J.I., Scheck-Wenderoth, M., 2016. A 3D gravity and thermal model for the Barents Sea and Kara Sea. Tectonophysics 684, 131-147, http://dx.doi.org/10.1016/j.tecto.2016.04.033.

Korenaga, J., Holbrook, W. S., Kent, G. M., Kelemen, P. B., Detrick, R. S., Larsen, H. C., Hopper, J. R., Dahl-Jensen, T., 2000. Crustal structure of the southeast Greenland margin from joint refraction and reflection seismic tomography. Journal of Geophysical Research 105, 21591-21614.

Krysiński, L., Grad, M., Mjelde, R., Czuba, W., Guterch, A., 2013. Seismic and density structure of the lithosphere-asthenosphere system along transect Knipovich Ridge-Spistbergen-Barents Sea – geological and petrophysical implications. Polish Polar Research 34 (2), 111-138, https://doi.org/10.2478/popore-2013-0011.

Leever, K. A., Gabrielsen, R H., Faleide, J. I, Braathen, A., 2011. A transpressional origin for the West Spitsbergen ford-and-trust belt: insight from analog modeling. Tectonics 30 (2), 10.1029/2010TC002753.

Manby, G., Lyberis, N., 1992. Tectonic evolution of the Devonian Basin of northern Svalbard. Norsk Geologisk Tidsskrift 72, 7-19.

Marello, L., Ebbing, J., Gernigon, L., 2010. Magnetic basement study in the Barents Sea from inversion and forward modelling. Tectonophysics 493, 153-171, 10.1016/j.tecto.2010.07.014.

Marello, L., Ebbing J., Gernigon, L., 2013. Basement inhomegenities and crustal setting in the Barents Sea from a combined 3D gravity and magnetic model. Geophys. J. Int. 193, 557-584, 10.1093/gji/ggt018.

Minakov, A., Mjelde, R., Faleide, J. I., Flueh, E. R., Dannowski, A., Keers, H., 2012. Mafic intrusions east of Svalbard imaged by active-source seismic tomography. Tectonophysics 518-521, 106-118, 10.1016/j.tecto.2011.11.015.

Minakov, A., Bretel, P., Lebedeva-Ivanova, N., Meyer, O., 2014. Cruise report: Barents OBS 2014, Ocean Bottom Survey In The Barents Sea, University of Oslo report, 35 pp.

Minakov, A. Yarushina, V., Faleide, J. I., Krupnova, N., Sakoulina, T., Dergunov, N., Glebovsky, V., 2017. Dyke emplacement and crustal structure within a continental large igneous province, northern Barents Sea. In: Pease, V., Coakley, B. (eds.) Circum-Arctic Lithosphere Evolution. Geological Society, London, Special Publications, 460, https://doi.org/10.1144/SP460.4.

Minshull, T. A., 2009. Geophysical characterisation of ocean-continent transition at magma-poor rifted margins. Comptes Rendus Geoscience 341 (5), 382-393, https://doi.org/10.1016/j.crte.2008.09.003.

Mjelde, R., Sellevoll, M. A., Shimamura, H., Iwasaki, T., Kanazawa, T., 1992. A crustal study off Lofoten, N. Norway, by use of 3-component ocean bottom seismographs. Tectonophysics 212, 269-288,

Mjelde, R., Sellevoll, M. A., 1993. Possible shallow crustal shear wave anisotropy off Lofoten, Norway, inferred from three-component ocean-bottom seismographs. Geophys. J. Int. 155 (1), 159-167, https://doi.org/10.1111/j.1365-246X.1993.tb05596.x

Mjelde, R., Sellevoll, M. A., Shimamura, H., Iwasaki, T., Kanazawa, T., 1993. Crustal structure under Lofoten, N. Norway, from vertical incidence and wide angle data. Geophys. J. Int. 114, 116-126, 10.1111/j.1365-246X.1993.tb01471.x

Mjelde, R., Myhre, B., Sellevoll, M.A., Shimamura, H., Iwasaki, T., Kanazawa, T., 1996. Modelling of S-waves from an area covered with flood-basalt off Lofoten, N. Norway. Geophs.Trans. 40, 95-117.

Mjelde, R., Fjellanger, J. P., Raum, T., Digranes, P., Kodira, S., Breivik, A., Shimamura, H., 2002. Where do P-S conversions occur? Analysis of OBS-data from the NE Atlantic Margin. First Break 20 (3), 10.1046/j.1365-2397.2002.00245.x.

Mjelde, R., Raum, T., Digranes, P., Shimamura, H., Shiobara, H., Kodaira, S., 2003. V_p/V_s ratio along the Vøring Margin, NE Atlantic, derived from OBS data: implications on lithology and stress field. Tectonophysics 369 (3-4), 175-197, https://doi.org/10.1016/S0040-1951(03)00198-7.

Neidell, N. S., 1985. Land application of S-waves. Geophys.: Lead. Edge of Explor. 11, 32-44.

Ottemöller, L., Kim, W. Y., Dallmann, W., Walderhauser, F., 2014. Storfjorden intraplate earthquake sequence, 2008-2014. (Unpublished).

Pease, V., Gee, D., Lopatin, B., 2001. Is Franz Josef Land affected by Caledonian deformation? European Union of Geosciences, Abstracts, 5, 757.

Pease, V. Drachev, S., Stephenson, R., Zhang, X., 2014. Arctic lithosphere – a review, Tectonophysics, 625, 1-25, https://doi.org/10.1016/j.tecto.2014.05.033.

Petersen, T. G., Thomsen, T. B., Olaussen, S., Stemmerik, L., 2016. Provenance shifts in an evolving Eurekan foreland basin: the Tertiary Central Basin, Spitsbergen. Journal of the Geological Society 173, 634-648, https://doi.org/10.1144/jgs2015-076.

Piepjohn, K., 2000. The Svalbardian-Ellesmerian deformation of the Old Red Sandstone and the pre-Devonian basement in NW Spitsbergen (Svalbard). In: Friend, P.F., Williams, B.P.J. (eds.), New Perspectives on the Old Red Sandstone. Geological Society of London Special Publications 180, 585-601.

Piepjohn, K., vonGossen, W., Tessensohn, F., 2016. The Eurekan deformation in the Arctic: an outline. Journal of the Geological Society 173, 1007-1024, https://doi.org/10.1144/jgs2016-081.

Pirli, M., Schweitzer, J., Paulsen, B., 2013. The Storfjorden, Svalbard, 2008-2012 aftershock sequence: Seismotectonics in a polar environment. Tectonophysics, 601, 192-205, https://doi.org/10.1016/j.tecto.2013.05.010.

Polteau, S., Hendriks, B. W. H., Planke, S., Ganerød, M., Corfu, F., Faleide, J. I., Midtkandal, I., Svensen, H. S., Myklebust, R., 2016. The Early Cretaceous Barents Sea Sill Complex: Distribution, $^{40}Ar/^{39}Ar$ geochronology, and implications for carbon gas formation. Palaeogeography, Palaeoclimatology, Palaeoecology 441, 83-95.

Pratt, R.G., 1999. Seismic waveform inversion in the frequency domain, Part 1: theory and verification in a physical scale model. Geophysics 64 (3), 888-901.

Ritzmann, O., Faleide, J. I., 2007. Caledonian basement of the western Barents Sea. Tectonics, 26 (5), 1-20, 10.1029/2006TC002059 TC5014.

Ritzmann, O., Faleide, J., I., 2009. The crust and mantle lithosphere in the Barents Sea/Kara Sea region. Tectonophysics 470, 89-104, https://doi.org/10.1016/j.tecto.2008.06.018.

Roberts, D., Gee, D. G., 1985. An introduction to the structure of the Scandinavian Caledonides. In: Gee, D.G., Sturt, B.A. (eds.) The Caledonide Orogen – Scandinavia and Related Areas. John Wiley & Sons, Chichester 55-68.

Skilbrei, J.R., 1992. Preliminary interpretation of aeromagnetic data from Spitsbergen, Svalbard Archipelagio (76°-79°N): implications for structure of the basement. Marine Geology 106, 53-68.

Smelror, M., Petrov, O., Larsen, G. B., Werner, S.C., 2009. Atlas: Geological History of the Barents Sea. Geological Survey of Norway, Trondheim.

Talwani, M., Eldholm, O., 1977. Evolution of the Norwegian-Greenland Sea. Geological Society of America Bulletin 88, 969-999.

Tarantola, A., 1984. Inversion of seismic reflection data in the acoustic approximation. Geophysics 49 (8), 1259-1266.

Tatham, R. H., 1985. Shear waves and lithology. In: Dohr, G. (ed.), Seismic Shear Waves: Part B. Applications. Geophysical Press, London, 86-133.

Tatham, R. H., McCormac, M. D., 1991. Rock physics measurements. In: Neizel, E. B., Winterstein, D. F. (eds.), Multicomponent Seismology in Petroleum Exploration. SEG Investigation in Geophysics Series, vol. 6. Society of Exploration Geophysicists.

Zelt, C. A., Smith, R.B., 1992. Seismic traveltime inversion from 2-D crustal velocity structure. Geophys. J. Int. 108, 16-34, https://doi.org/10.1111/j.1365-246X.1992.tb00836.x

Wilson, J. T., 1972. Continents adrift. Readings from Scientific American Freeman WH and Company, San Francisco, 172 p.

Worsley, D., 2008. The post-Caledonian development of Svalbard and the western Barents Sea. Polar Res. 27, 298-317, 10.1111/j.1751-8369.2008.00085.x.

Graphic design: Communication Division, UiB / Print: Skipnes Kommunikasjon AS

uib.no

ISBN: 978-82-308-3759-7